

# Performance Analysis and Design of Maximum Ratio Combining in Channel-Aware MIMO Decision Fusion

Domenico Ciuonzo, *Student Member, IEEE*, Gianmarco Romano, *Member, IEEE*,  
and Pierluigi Salvo Rossi, *Senior Member, IEEE*

**Abstract**—In this paper we present a theoretical performance analysis of the maximum ratio combining (MRC) rule for channel-aware decision fusion over multiple-input multiple-output (MIMO) channels for (conditionally) dependent and independent local decisions. The system probabilities of false alarm and detection conditioned on the channel realization are derived in closed form and an approximated threshold choice is given. Furthermore, the channel-averaged (CA) performances are evaluated in terms of the CA system probabilities of false alarm and detection and the area under the receiver operating characteristic (ROC) through the closed form of the conditional moment generating function (MGF) of the MRC statistic, along with Gauss-Chebyshev (GC) quadrature rules. Furthermore, we derive the deflection coefficients in closed form, which are used for sensor threshold design. Finally, all the results are confirmed through Monte Carlo simulations.

**Index Terms**—Decision fusion, distributed detection, MIMO, MRC, wireless sensor networks.

## I. INTRODUCTION

### A. Motivation and Related Works

OPTIMUM channel-aware decision fusion (DF) in wireless sensor networks (WSNs) with instantaneous channel-state information (CSI) is a challenging task and, due to the numerical instability and strong requirements on the system knowledge required by the log-likelihood ratio (LLR) test, several sub-optimal alternatives have been analyzed in the recent literature, such as maximum ratio combining (MRC), equal gain combining and Chair-Varshney maximum likelihood [1], [2]. Max-Log rule has been studied in [3] and shown to outperform other sub-optimal rules though exhibiting higher complexity and requirements on system knowledge, e.g. the channel variance. All the mentioned rules were derived in the parallel-access channel (PAC) scenario and, for such a case, a theoretical performance analysis was also conducted in [3].

Recently, DF exploiting the interfering nature of the broadcast wireless medium is becoming more attractive for spectral-efficiency purposes. Distributed detection over a multiple-access channel (MAC) is studied in [4], where perfect compensation of the fading coefficients is assumed for each sensor. Non-coherent modulation and censoring over PAC and MAC have been analyzed in [5] with emphasis on processing gain

and combining loss. The same scenario is studied in [6], with a focus on the error exponents (obtained through the large deviation principle) and the design of energy-efficient modulations for Rayleigh and Rice fading. Optimality of received-energy statistic in Rayleigh fading scenario is demonstrated for a diversity MAC with non-identical sensors in [7]. Efficient DF over MAC only with knowledge of the instantaneous channel gains and with the help of power-control and phase-shifting techniques is studied in [8]. Techniques borrowed from direct-sequence spread-spectrum systems are combined with on-off keying (OOK) modulation and censoring for DF in scenarios with statistical CSI [9].

DF with a multiple-input multiple-output (MIMO) wireless channel model has been first studied in [10], with a focus on power-allocation design based on instantaneous CSI, under the framework of J-divergence. Distributed detection with ultra-wideband sensors over MAC has been then studied in [11]; the same model was adopted to study data fusion over MIMO channels with amplify and forward sensors in [12].

Various sub-optimal fusion rules (with reduced system knowledge) for channel-aware DF in the MIMO scenario with instantaneous CSI have been proposed in [13], where decode-and-fuse and decode-then-fuse approaches are compared through simulation results. It is worth noticing that in such scenario the LLR is not a viable solution, since it suffers from the exponential growth of the computational complexity with respect to (w.r.t.) the number of sensors and high required system knowledge.

Differently, it has been shown that the MRC (sub-optimal) fusion rule in MIMO scenario has the following appealing properties [13]: (i) it exploits efficiently diversity from multiple antennas; (ii) it achieves optimality at low signal-to-noise ratio (SNR); (iii) its complexity is linear w.r.t. the number of antennas and independent of the number of sensors, both in the fusion and channel estimation stages; (iv) it requires only limited system knowledge. Unfortunately, MRC performance was (partially) assessed by relying on time-consuming Monte Carlo (MC) simulations. Also, (i) no explicit formula for the choice of the threshold for the MRC fusion rule, assuring a given false-alarm rate, was derived, (ii) no theoretical results on the dependence of such fusion rule w.r.t. the WSN parameters (i.e. the local-sensor performance, the channel SNR, the number of sensors and the number of antennas) were presented and (iii) an asymptotic analysis w.r.t. the mentioned parameters was lacking.

The authors are with the Department of Industrial and Information Engineering, Second University of Naples, Aversa (CE), Italy. Email: {domenico.ciuonzo, gianmarco.romano, pierluigi.salvorossi}@unina2.it.

## B. Main Results and Paper Organization

The main contributions of this manuscript are related to the MRC fusion rule over MIMO channel and are summarized as follows:

- We obtain the closed form expressions of the instantaneous-channel (IC) system probabilities of false alarm and detection, that are exploited to: (i) derive an approximate expression for the system threshold in order to approach a target false-alarm rate, under *low-SNR and large-system* (i.e. a high number of sensors) regime; (ii) evaluate the IC system probabilities of false alarm and detection under a *large antenna array* (i.e. a high number of antennas) regime at the DF center (DFC).
- We derive the closed form expression of the channel-averaged (CA) conditional moment generating function (MGF) of the statistic, i.e. averaged over the statistical distribution of the channel; such a result is used in conjunction with Gauss-Chebyshev (GC) quadrature rules to *efficiently* evaluate the CA probability of detection and false alarm, as opposed to the results obtained via (time consuming) MC simulations in [13]; the obtained result is very general, as it holds for scenarios with both (conditionally) dependent and independent local decisions.
- The CA conditional MGF is exploited to show that large-system limit under both individual power constraint (IPC) and total power constraint (TPC) scenarios *leads to a non-ideal receiver operating characteristic (ROC)* in both cases. Such a result allows: (i) to claim zero error-exponents; (ii) a convenient evaluation of maximum achievable performance with a fixed number of antennas (and a fixed SNR under TPC).
- The CA conditional MGF is used in a new general formula for GC-based computation of the *area under the ROC* (AUC), thus allowing synthetic and global performance analysis of the statistic.
- Finally, we derive explicitly the (modified) deflection coefficient [14], which is exploited in order to obtain a convenient choice of the local threshold; the effectiveness of this approach is confirmed via simulations.

The manuscript is organized as follows: Section II introduces the system model, while in Section III we recall the LLR and the MRC rules for the model under investigation; in Section IV we present the theoretical results needed for the performance analysis of MRC, while some guidelines on the system design with MRC are obtained in Section V, via the deflection coefficients; the results are verified and analyzed in Section VI; finally in Section VII we draw some concluding remarks; proofs and derivations are confined to the Appendices.

*Notation* - Lower-case (resp. Upper-case) bold letters denote vectors (resp. matrices), with  $a_n$  (resp.  $a_{n,m}$ ) representing the  $n$ th (resp. the  $(n,m)$ th) element of  $\mathbf{a}$  (resp.  $\mathbf{A}$ ); upper-case calligraphic letters denote finite sets, with  $\mathcal{A}^K$  representing the  $k$ -ary Cartesian power of  $\mathcal{A}$ ;  $\mathbf{I}_N$  denotes the  $N \times N$  identity matrix;  $\mathbf{0}_N$  (resp.  $\mathbf{1}_N$ ) denotes the null (resp. ones) vector of length  $N$ ;  $\mathbb{E}\{\cdot\}$ ,  $\text{var}\{\cdot\}$ ,  $(\cdot)^t$ ,  $(\cdot)^\dagger$ ,  $\Re(\cdot)$ ,  $\Im(\cdot)$ ,  $\|\cdot\|$  and  $\det(\cdot)$  denote expectation, variance, transpose, conjugate

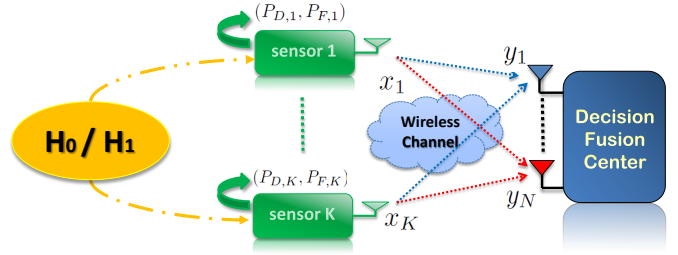


Figure 1: The DF model in presence of a (virtual) MIMO channel.

transpose, real part, imaginary part, Frobenius norm and matrix determinant operators, respectively;  $j$  denotes the imaginary unit;  $P(\cdot)$  and  $p(\cdot)$  denote probability mass functions (pmf) and probability density functions (pdf), while  $P(\cdot|\cdot)$  and  $p(\cdot|\cdot)$  their corresponding conditional counterparts;  $\mathcal{N}_{\mathbb{C}}(\boldsymbol{\mu}, \boldsymbol{\Sigma})$  (resp.  $\mathcal{N}(\boldsymbol{\mu}, \boldsymbol{\Sigma})$ ) denotes a circularly symmetric complex (resp. real) normal distribution with mean vector  $\boldsymbol{\mu}$  and covariance matrix  $\boldsymbol{\Sigma}$ , while  $\mathcal{Q}(\cdot)$  is the complementary cumulative distribution function of a standard normal distribution;  $\mathcal{B}(k, p)$  denotes a binomial distribution of  $k$  trials with probability of success  $p$ ;  $\Gamma(k, \theta)$  denotes a Gamma distribution with shape parameter  $k$  and scale parameter  $\theta$ ; finally the symbols  $\propto$ ,  $\rightarrow$ ,  $\xrightarrow{d}$  and  $\sim$  mean “proportional to”, “tends to”, “tends in distribution to” and “distributed as”, respectively.

## II. SYSTEM MODEL

In this section we briefly describe the system model, illustrated in Fig. 1. We consider a distributed binary hypothesis test, where  $K$  sensors are used to discriminate between the hypotheses of the set  $\mathcal{H} \triangleq \{\mathcal{H}_0, \mathcal{H}_1\}$ . For example  $\mathcal{H}_0$  and  $\mathcal{H}_1$  may represent the absence and the presence of a specific target of interest, respectively. The  $k$ th sensor,  $k \in \mathcal{K} \triangleq \{1, 2, \dots, K\}$ , takes a binary local decision  $d_k \in \mathcal{H}$  about the observed phenomenon on the basis of its own measurements. Here *we do not make any conditional* (given  $\mathcal{H}_i \in \mathcal{H}$ ) *mutual independence assumption* on  $d_k$ . Each decision  $d_k$  is mapped to a symbol  $x_k \in \mathcal{X} = \{-1, +1\}$  representing a binary phase-shift keying (BPSK) modulation<sup>1</sup>: without loss of generality (w.l.o.g.) we assume that  $d_k = \mathcal{H}_i$  maps into  $x_k = 2i - 1$ ,  $i \in \{0, 1\}$ . The quality of the  $k$ th sensor decisions is characterized by the conditional probabilities  $P(x_k|\mathcal{H}_i)$ . More specifically, we denote  $P_{D,k} \triangleq P(x_k = 1|\mathcal{H}_1)$  and  $P_{F,k} \triangleq P(x_k = 1|\mathcal{H}_0)$  the probability of detection and false alarm of the  $k$ th sensor, respectively.

Sensors communicate with DFC over a wireless flat-fading MAC, with independent and identically distributed (i.i.d.) Rayleigh fading coefficients of unitary mean power. The DFC is equipped with  $N$  receive antennas in order to exploit diversity and combat signal attenuation due to small-scale fading; this configuration determines a distributed or “virtual” MIMO channel [10], [13]. Also, instantaneous CSI and perfect

<sup>1</sup>In the case of an absence/presence task, where  $\mathcal{H}_0$  is much more probable, OOK can be employed for energy-efficiency purposes. Hereinafter we will refer only to BPSK, however the results apply readily to OOK.

synchronization<sup>2</sup> are assumed at the DFC as in [4], [7], [10], [13].

We denote:  $y_n$  the received signal at the  $n$ th receive antenna of the DFC after matched filtering and sampling;  $h_{n,k} \sim \mathcal{N}_{\mathbb{C}}(0, 1)$  the fading coefficient between the  $k$ th sensor and the  $n$ th receive antenna of the DFC;  $w_n$  the additive white Gaussian noise at the  $n$ th receive antenna of the DFC. The vector model at the DFC is the following:

$$\mathbf{y} = \mathbf{H}\mathbf{x} + \mathbf{w} \quad (1)$$

where  $\mathbf{y} \in \mathbb{C}^N$ ,  $\mathbf{H} \in \mathbb{C}^{N \times K}$ ,  $\mathbf{x} \in \mathcal{X}^K$ ,  $\mathbf{w} \sim \mathcal{N}_{\mathbb{C}}(\mathbf{0}_N, \sigma_w^2 \mathbf{I}_N)$  are the received-signal vector, the channel matrix, the transmitted-signal vector and the noise vector, respectively. Furthermore, we define the random variable (r.v.)  $\ell(\mathbf{x})$  denoting the number of sensors deciding  $\mathcal{H}_1$  and the set  $\mathcal{L} \triangleq \{0, \dots, K\}$ , denoting the outcomes of  $\ell(\mathbf{x})$ .

Finally, we define the total channel SNR as the ratio between the energy transmitted from the WSN  $\mathcal{E}_s \triangleq \mathbb{E}\{\|\mathbf{x}\|^2\} = K$  and the one-sided power spectral density of the noise  $\sigma_w^2$ , i.e.  $\text{SNR} \triangleq \frac{\mathcal{E}_s}{\sigma_w^2} = \frac{K}{\sigma_w^2}$ ; therefore the individual channel SNR for the  $k$ th sensor will be  $\text{SNR}_* = \frac{1}{\sigma_w^2}$ . Hereinafter we will consider in our analysis both IPC (i.e. fixed  $\text{SNR}_*$ ) and TPC (i.e. fixed SNR) on the WSN.

### III. FUSION RULES

#### A. Optimum Rule

The optimal test [15] for the considered problem is formulated as

$$\Lambda_{opt} \triangleq \ln \left[ \frac{p(\mathbf{y}|\mathbf{H}, \mathcal{H}_1)}{p(\mathbf{y}|\mathbf{H}, \mathcal{H}_0)} \right] \underset{\hat{\mathcal{H}}=\mathcal{H}_0}{\overset{\hat{\mathcal{H}}=\mathcal{H}_1}{\geq}} \gamma \quad (2)$$

where  $\hat{\mathcal{H}}$ ,  $\Lambda_{opt}$  and  $\gamma$  denote the estimated hypothesis, the LLR and the threshold which the LLR is compared to. The threshold  $\gamma$  can be determined to assure a fixed system false-alarm rate (Neyman-Pearson approach), or can be chosen to minimize the probability of error (Bayesian approach) [15]. Exploiting the independence<sup>3</sup> of  $\mathbf{y}$  from  $\mathcal{H}_i$ , given  $\mathbf{x}$ , an explicit expression of the LLR from Eq. (2) is given by

$$\begin{aligned} \Lambda_{opt} &= \ln \left[ \frac{\sum_{\mathbf{x} \in \mathcal{X}^K} p(\mathbf{y}|\mathbf{H}, \mathbf{x}) P(\mathbf{x}|\mathcal{H}_1)}{\sum_{\mathbf{x} \in \mathcal{X}^K} p(\mathbf{y}|\mathbf{H}, \mathbf{x}) P(\mathbf{x}|\mathcal{H}_0)} \right] \\ &= \ln \left[ \frac{\sum_{\mathbf{x} \in \mathcal{X}^K} \exp\left(-\frac{\|\mathbf{y} - \mathbf{H}\mathbf{x}\|^2}{\sigma_w^2}\right) P(\mathbf{x}|\mathcal{H}_1)}{\sum_{\mathbf{x} \in \mathcal{X}^K} \exp\left(-\frac{\|\mathbf{y} - \mathbf{H}\mathbf{x}\|^2}{\sigma_w^2}\right) P(\mathbf{x}|\mathcal{H}_0)} \right]. \end{aligned} \quad (3)$$

Unfortunately, the optimal rule in Eq. (3) presents several difficulties in the implementation: (i) complete knowledge of  $\mathbf{H}$ ,  $P(\mathbf{x}|\mathcal{H}_i)$  and  $\sigma_w^2$ ; (ii) numerical instability of the expression, due to the presence of exponential functions with large dynamics [3], [13]; (iii) exponential growth of the complexity with  $K$ . Design of sub-optimal DF rules with simpler implementation and reduced system knowledge is then extremely desirable.

<sup>2</sup>Multiple antennas at the DFC do not make these assumptions harder to verify w.r.t. a single-antenna MAC.

<sup>3</sup>In fact, as shown in Fig. 1, the directed triple formed by hypothesis, the transmitted-signal vector and the received-signal vector satisfies the Markov property.

#### B. MRC

The LLR of Eq. (3) can be simplified under the assumption of perfect sensors [3], [9], i.e.  $P(\mathbf{x} = \mathbf{1}_K|\mathcal{H}_1) = P(\mathbf{x} = -\mathbf{1}_K|\mathcal{H}_0) = 1$ . In this case  $\mathbf{x} \in \{\mathbf{1}_K, -\mathbf{1}_K\}$  and Eq. (3) reduces to [13]:

$$\ln \left[ \frac{\exp\left(-\frac{\|\mathbf{y} - \mathbf{H}\mathbf{1}_K\|^2}{\sigma_w^2}\right)}{\exp\left(-\frac{\|\mathbf{y} + \mathbf{H}\mathbf{1}_K\|^2}{\sigma_w^2}\right)} \right] \propto \Re(\mathbf{z}_{MRC}^\dagger \mathbf{y}) \triangleq \Lambda_{MRC} \quad (4)$$

with  $\mathbf{z}_{MRC} \triangleq \mathbf{H}\mathbf{1}_K$

where terms independent on  $\mathbf{y}$  have been incorporated in  $\gamma$  as in Eq. (2). It is worth noticing that the MRC is a *sub-optimal* rule since, in the practice, the sensor local decisions are far from being perfect. However, it has been proved in [13] that MRC is the low-SNR approximation of the optimum of Eq. (3) when local performances of sensors are identical<sup>4</sup>. Furthermore, as stated in the introduction, its computational complexity is independent of  $K$  in both fusion and channel-estimation stages, since  $\mathbf{z}_{MRC} = \mathbf{H}\mathbf{1}_K$  (which is the only required parameter for the rule implementation, as opposed to the LLR) can be directly estimated<sup>5</sup> and used in Eq. (4).

### IV. MRC PERFORMANCE ANALYSIS

#### A. IC False Alarm and Detection probabilities and threshold computation

The IC system probabilities of false alarm and detection are defined as

$$P_{F_0}(\mathbf{H}, \gamma) \triangleq P(\Lambda > \gamma | \mathbf{H}, \mathcal{H}_0), \quad (5)$$

$$P_{D_0}(\mathbf{H}, \gamma) \triangleq P(\Lambda > \gamma | \mathbf{H}, \mathcal{H}_1), \quad (6)$$

with  $\Lambda$  representing the decision statistic of a generic fusion rule. It is shown in Appendix A that

$$\Lambda_{MRC} | \mathbf{H}, \mathcal{H}_i \sim \sum_{\mathbf{x} \in \mathcal{X}^K} P(\mathbf{x}|\mathcal{H}_i) \mathcal{N}\left(\Re(\mathbf{z}_{MRC}^\dagger \mathbf{H}\mathbf{x}), \frac{\sigma_w^2}{2} \|\mathbf{z}_{MRC}\|^2\right), \quad (7)$$

i.e. the pdf  $p_{\Lambda_{MRC}}(\lambda | \mathbf{H}, \mathcal{H}_i)$ ,  $\lambda \in \mathbb{R}$ ,  $\mathcal{H}_i \in \mathcal{H}$ , is a *Gaussian mixture*. Therefore, combining Eqs. (5), (6) and (7), leads to:

$$P_{F_0}(\mathbf{H}, \gamma) = \sum_{\mathbf{x} \in \mathcal{X}^K} P(\mathbf{x}|\mathcal{H}_0) \mathcal{Q}\left(\frac{\gamma - \Re(\mathbf{z}_{MRC}^\dagger \mathbf{H}\mathbf{x})}{\sqrt{\frac{1}{2}\sigma_w \|\mathbf{z}_{MRC}\|}}\right); \quad (8)$$

$$P_{D_0}(\mathbf{H}, \gamma) = \sum_{\mathbf{x} \in \mathcal{X}^K} P(\mathbf{x}|\mathcal{H}_1) \mathcal{Q}\left(\frac{\gamma - \Re(\mathbf{z}_{MRC}^\dagger \mathbf{H}\mathbf{x})}{\sqrt{\frac{1}{2}\sigma_w \|\mathbf{z}_{MRC}\|}}\right). \quad (9)$$

The explicit expression of  $P_{F_0}(\mathbf{H})$  in Eq. (8) cannot be easily used to design a threshold  $\gamma$  which satisfies a given false-alarm

<sup>4</sup>Even if in [13] conditional mutual independence of local decisions was assumed, it can be shown by inspection of the derivation that such an assumption is not necessary in proving MRC optimality at low-SNR.

<sup>5</sup>This is easily obtained with a channel estimation procedure in which all the sensors transmit  $x_k = 1$  (or equivalently  $x_k = -1$ ). However, time-varying channels in high-mobility scenarios may be problematic as the channel state information could be outdated when available [16].

rate, since a two-fold complication is present: (i) the inversion can be done only numerically and requires the evaluation of a sum over  $2^K$  terms; (ii) complete knowledge of  $\mathbf{H}$  (and not of only  $\mathbf{z}_{MRC} = \mathbf{H}\mathbf{1}_K$ , as required instead from the MRC rule),  $P(\mathbf{x}|\mathcal{H}_0)$  and  $\sigma_w^2$  is required.

Nonetheless, a low-SNR large-system ( $K \rightarrow +\infty$ ) approximation of  $\gamma$  with reduced system knowledge can be found, given a target  $\check{P}_{F_0}$ ; the result is stated by the following proposition, in the case of (conditionally) uncorrelated sensor decisions (under  $\mathcal{H}_0$ ) and  $P_{F,k} = P_F$ ,  $k \in \mathcal{K}$ .

**Proposition 1.** *Assuming (i)  $\mathbb{E}\{\mathbf{x}|\mathcal{H}_0\} = \boldsymbol{\mu}_0 \triangleq (2P_F - 1)\mathbf{1}_K$  and (ii)  $\mathbb{E}\{(\mathbf{x} - \boldsymbol{\mu}_0)(\mathbf{x} - \boldsymbol{\mu}_0)^T|\mathcal{H}_0\} = [1 - (2P_F - 1)^2] \cdot \mathbf{I}_K$ , a low-SNR large-system  $\check{\gamma}$  for approaching a target  $\check{P}_{F_0}$ , is given by*

$$\check{\gamma} \triangleq \mathcal{Q}^{-1}(\check{P}_{F_0}) \sqrt{\frac{(1 - \delta^2)K + \sigma_w^2}{2}} \|\mathbf{z}_{MRC}\| + \delta \|\mathbf{z}_{MRC}\|^2 \quad (10)$$

where  $\delta \triangleq (2P_F - 1)$ .

*Proof:* The proof is given in Appendix A.  $\blacksquare$

The accuracy of Eq. (10) will be verified in Section VI; it is worth noticing that such expression *does not require* the complete knowledge of  $\mathbf{H}$  (the dependence is only through  $\mathbf{z}_{MRC} = \mathbf{H}\mathbf{1}_K$ ) and  $P(\mathbf{x}|\mathcal{H}_0)$ . Also, the assumptions on  $P(\mathbf{x}|\mathcal{H}_0)$  in Proposition 1 are generally verified when the local threshold at each sensor is set up to satisfy the same false-alarm rate (assumption (i)) and the local decisions are *uncorrelated* under the hypothesis  $\mathcal{H}_0$  (assumption (ii)), which is typically the case when  $\mathcal{H}_0$  corresponds to the absence of an event of interest.

Furthermore, it can be shown that for large  $N$  at the DFC, Eq. (7) reduces to

$$\Lambda_{MRC} | \mathbf{H}, \mathcal{H}_i \stackrel{\text{approx.}}{\sim} \sum_{\mathbf{x} \in \mathcal{X}^K} P(\mathbf{x}|\mathcal{H}_i) \mathcal{N} \left( (2\ell(\mathbf{x}) - K)N, \frac{\sigma_w^2}{2}NK \right) = \quad (11)$$

$$\sum_{\ell(\mathbf{x})=0}^K P(\ell(\mathbf{x})|\mathcal{H}_i) \mathcal{N} \left( (2\ell(\mathbf{x}) - K)N, \frac{\sigma_w^2}{2}NK \right), \quad (12)$$

since, when  $N$  is large, the approximation  $\mathbf{H}^\dagger \mathbf{H} \approx N\mathbf{I}_K$  holds [17]. It is worth noticing that a large antenna array at the DFC on one hand makes the performance independent of the particular instance of  $\mathbf{H}$ , on the other hand it “reduces” the dependence of the MRC performances w.r.t. the (joint) sensor performance, i.e. requires only  $P(\ell(\mathbf{x})|\mathcal{H}_i)$  as opposed to  $P(\mathbf{x}|\mathcal{H}_i)$  (cf. Eq. (7)). This result is confirmed by observing that, for large  $N$ , Eq. (4) reduces to

$$\Lambda_{MRC} \approx N \cdot \sum_{k=1}^K x_k + \Re\{\bar{w}\}, \quad (13)$$

where  $\bar{w} \sim \mathcal{N}_{\mathbb{C}}(0, \sigma_w^2 NK)$ , i.e. the MRC approaches a “noisy” counting rule [18].

## B. CA False Alarm and Detection probabilities

The CA system probabilities of false alarm and detection are

$$P_{F_0}(\gamma) \triangleq \mathbb{E}_{\mathbf{H}}\{P_{F_0}(\gamma, \mathbf{H})\} = P(-\Lambda < -\gamma|\mathcal{H}_0), \quad (14)$$

$$P_{D_0}(\gamma) \triangleq \mathbb{E}_{\mathbf{H}}\{P_{D_0}(\gamma, \mathbf{H})\} = P(-\Lambda < -\gamma|\mathcal{H}_1), \quad (15)$$

with  $\Lambda$  representing the decision statistic of a generic fusion rule. It is worth noticing that Eqs. (14) and (15) are formulated in terms of  $-\Lambda$  in order to exploit readily the standard definition of the conditional MGFs in the Laplace domain [3]. Although it is often difficult to derive the conditional pdf  $p_{-\Lambda}(\lambda|\mathcal{H}_i)$ ,  $\lambda \in \mathbb{R}$ ,  $\mathcal{H}_i \in \mathcal{H}$ , of the r.v.  $-\Lambda$ , the corresponding Laplace transform  $\Phi_{-\Lambda}(s|\mathcal{H}_i)$  (i.e. the MGF of  $\Lambda|\mathcal{H}_i$ ) is usually easier to obtain. Using the relationship  $p_{-\Lambda}(\lambda|\mathcal{H}_i) = \frac{1}{2\pi j} \int_{c-j\infty}^{c+j\infty} \Phi_{-\Lambda}(s|\mathcal{H}_i) \exp(\lambda s) ds$ , where  $c$  is a small (positive) constant in the region of convergence (RC) of the integral, both probabilities in Eqs. (14) and (15) can be rewritten as

$$\int_{-\infty}^{-\gamma} p_{-\Lambda}(\lambda|\mathcal{H}_i) d\lambda = \int_{c-j\infty}^{c+j\infty} \Phi_{-\Lambda}(s|\mathcal{H}_i) \frac{\exp(-\gamma s)}{2\pi j} \frac{ds}{s}. \quad (16)$$

Based on Eq. (16),  $P_{F_0}(\gamma)$  and  $P_{D_0}(\gamma)$  can be calculated for any fusion rule provided that the integral in Eq. (16) can be solved efficiently and the corresponding Laplace transform  $\Phi_{-\Lambda}(s|\mathcal{H}_i)$  can be derived in closed form. It is worth remarking that the same approach was used to efficiently evaluate CA probabilities of sub-optimal fusion rules over PAC in [3].

The integral in Eq. (16) can be solved exactly using the residue approach or numerically through GC quadrature rules [19], [20], [21]. Unfortunately, the former approach becomes long and intricate when poles of algebraic multiplicity greater than one are present (indeed this is our case, since we are considering multiple antennas at the DFC) [21]. On the other hand, following the latter approach, a direct application of the results in [19] to Eq. (16) leads to

$$\int_{-\infty}^{-\gamma} p_{-\Lambda}(\lambda|\mathcal{H}_i) d\lambda \approx \frac{1}{\nu} \sum_{r=1}^{\nu/2} [\Re(\varphi_i(r)) + \tau_r \cdot \Im(\varphi_i(r))], \quad (17)$$

$$\varphi_i(r) \triangleq \Phi_{-\Lambda}(\mu_r|\mathcal{H}_i) \exp(-\gamma \cdot \mu_r), \quad (18)$$

where  $\nu$  denotes the (even) number of nodes of the GC rules (i.e. the order of the approximation accuracy),  $\mu_r \triangleq c + jc\tau_r$  and  $\tau_r \triangleq \tan\left(\frac{(2r-1)\pi}{2\nu}\right)$ .

Differently, given the assumptions of the model under consideration,  $\Phi_{-\Lambda}(s|\mathcal{H}_i)$  can be expanded as

$$\Phi_{-\Lambda}(s|\mathcal{H}_i) = \sum_{\mathbf{x} \in \mathcal{X}^K} \Phi_{-\Lambda}(s|\mathbf{x}) P(\mathbf{x}|\mathcal{H}_i), \quad \mathcal{H}_i \in \mathcal{H}. \quad (19)$$

We derive here  $\Phi_{-\Lambda_{MRC}}(s|\mathbf{x})$  in closed form, as summarized by the following proposition.

**Proposition 2.** *The Laplace Transform  $\Phi_{-\Lambda_{MRC}}(s|\mathbf{x})$  of  $p_{-\Lambda_{MRC}}(\lambda|\mathbf{x})$  is given in closed form in Eq. (20) at the top of the next page, where  $\xi^+ \triangleq 1 + \sqrt{1 + \frac{1}{\text{SNR}}}$  and  $\xi^- \triangleq 1 - \sqrt{1 + \frac{1}{\text{SNR}}}$ .*

$$\Phi_{-\Lambda_{MRC}}(s|\mathbf{x}) = \frac{1}{\left\{ \left[ 1 + \frac{1}{2} (K \cdot \xi^+ - 2\ell(\mathbf{x})) s \right] \left[ 1 + \frac{1}{2} (K \cdot \xi^- - 2\ell(\mathbf{x})) s \right] \right\}^N}. \quad (20)$$

*Proof:* The proof is given in Appendix B. ■

It is worth noticing that, in the particular case of the MRC rule, Eq. (20) depends on  $\mathbf{x}$  only through  $\ell(\mathbf{x})$ , i.e.  $\Phi_{-\Lambda_{MRC}}(s|\mathbf{x}) = \Phi_{-\Lambda_{MRC}}(s|\ell(\mathbf{x}))$ . Then Eq. (19) is replaced efficiently with

$$\Phi_{-\Lambda_{MRC}}(s|\mathcal{H}_i) = \sum_{\ell(\mathbf{x})=0}^K \Phi_{-\Lambda_{MRC}}(s|\ell(\mathbf{x})) P(\ell(\mathbf{x})|\mathcal{H}_i), \quad (21)$$

requiring only a sum over  $(K+1)$  terms ( $\ell(\mathbf{x}) \in \mathcal{L}$ ), as opposed to  $2^K$  (cf. with Eq. (19)). Also, only  $P(\ell(\mathbf{x})|\mathcal{H}_i)$ , in the place of  $P(\mathbf{x}|\mathcal{H}_i)$ , is needed to evaluate  $\Phi_{-\Lambda_{MRC}}(s|\mathcal{H}_i)$ .

*Remarks:* from inspection of Eqs. (20) and (21), it can be shown that the RC of  $\Phi_{-\Lambda_{MRC}}(s|\mathcal{H}_i)$  is a vertical strip delimited by the axes determined by  $\Re(s) = \pm \frac{2}{K+K\sqrt{1+\frac{1}{\text{SNR}}}}$ .

### C. Large-system analysis

Taking a closer look at Eqs. (20) and (21) the large-system ( $K \rightarrow +\infty$ ) behaviour of the MRC under both IPC and TPC is not apparent. Such behaviour is put in evidence by the following proposition for the statistic<sup>6</sup>  $\tilde{\Lambda} \triangleq \frac{\Lambda_{MRC}}{K}$ , in the case of conditionally i.i.d. sensor decisions.

**Proposition 3.** *If  $P(\mathbf{x}|\mathcal{H}_i) = \prod_{k=1}^K P(x_k|\mathcal{H}_i)$ ,  $\mathcal{H}_i \in \mathcal{H}$ , and  $(P_{D,k}, P_{F,k}) = (P_D, P_F)$ ,  $k \in \mathcal{K}$ , as  $K \rightarrow +\infty$ , the Laplace transform  $\bar{\Phi}_{-\tilde{\Lambda}}(s|\mathcal{H}_i)$  of  $p_{-\tilde{\Lambda}}(\lambda|\mathcal{H}_i)$ , in the IPC scenario is given by:*

$$\bar{\Phi}_{-\tilde{\Lambda}}^I(s|\mathcal{H}_1) = \frac{1}{\left\{ [1 + (1 - P_D) s] [1 - P_D s] \right\}^N}; \quad (22)$$

$$\bar{\Phi}_{-\tilde{\Lambda}}^I(s|\mathcal{H}_0) = \frac{1}{\left\{ [1 + (1 - P_F) s] [1 - P_F s] \right\}^N}. \quad (23)$$

Correspondingly, as  $K \rightarrow +\infty$ ,  $\bar{\Phi}_{-\tilde{\Lambda}}(s|\mathcal{H}_i)$  in the TPC scenario is given by:

$$\bar{\Phi}_{-\tilde{\Lambda}}^T(s|\mathcal{H}_1) = \quad (24)$$

$$\frac{1}{\left\{ \left[ 1 + \frac{1}{2} (\xi^+ - 2P_D) s \right] \left[ 1 + \frac{1}{2} (\xi^- - 2P_D) s \right] \right\}^N}$$

$$\bar{\Phi}_{-\tilde{\Lambda}}^T(s|\mathcal{H}_0) = \quad (25)$$

$$\frac{1}{\left\{ \left[ 1 + \frac{1}{2} (\xi^+ - 2P_F) s \right] \left[ 1 + \frac{1}{2} (\xi^- - 2P_F) s \right] \right\}^N}$$

*Proof:* The proof is given in Appendix C. ■

*Remarks:* from inspection of Eq. (22) (resp. Eq. (23)), it can be shown that the RC of  $\bar{\Phi}_{-\tilde{\Lambda}}^I(s|\mathcal{H}_1)$  (resp.  $\bar{\Phi}_{-\tilde{\Lambda}}^I(s|\mathcal{H}_0)$ ) is a vertical strip delimited by the axes determined by  $\Re(s) = -\left(\frac{1}{1-P_D}\right)$  (resp.  $\Re(s) = -\left(\frac{1}{1-P_F}\right)$ ) and  $\Re(s) = \frac{1}{P_D}$  (resp.  $\Re(s) = \frac{1}{P_F}$ ). Differently,  $\bar{\Phi}_{-\tilde{\Lambda}}^T(s|\mathcal{H}_1)$  (resp.  $\bar{\Phi}_{-\tilde{\Lambda}}^T(s|\mathcal{H}_0)$ ) in

<sup>6</sup>Note that considering  $\tilde{\Lambda}$ , in the place of  $\Lambda_{MRC}$ , does not change MRC performance, since every positive constant can be absorbed by the threshold  $\gamma$  through Eq. (2). Nonetheless, the scaling factor  $1/K$  is added in order to assure convergence of the limit  $K \rightarrow +\infty$  for the MGFs being considered.

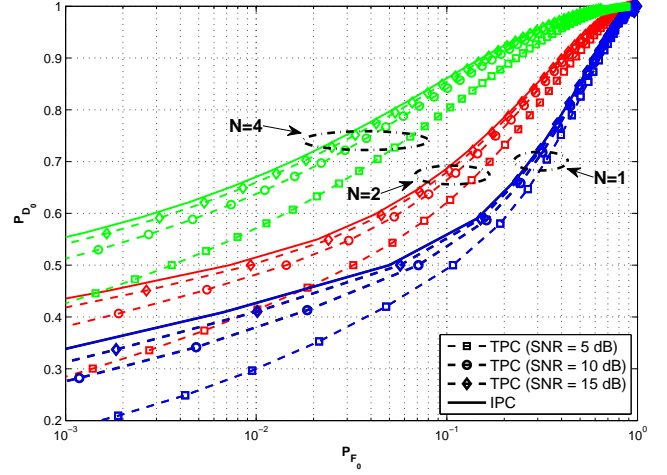


Figure 2: Large system ( $K \rightarrow +\infty$ ) ROC for conditionally i.i.d. sensor decisions in IPC and TPC case ( $(\text{SNR})_{\text{dB}} \in \{5, 10, 15\}$ );  $(P_{D,k}, P_{F,k}) = (0.5, 0.05)$ ,  $k \in \mathcal{K}$ .

Eq. (24) (resp. Eq. (25)) has a RC which is a vertical-strip delimited by the axes determined by  $\Re(s) = \frac{2}{2P_D - \xi^+}$  (resp.  $\Re(s) = \frac{2}{2P_F - \xi^+}$ ) and  $\Re(s) = \frac{2}{2P_D - \xi^-}$  (resp.  $\Re(s) = \frac{2}{2P_F - \xi^-}$ ).

In Fig. 2 it is illustrated the large-system CA-ROC, i.e.  $P_{D_0}$  vs  $P_{F_0}$ , obtained through the GC rules (with  $\nu = 10^3$ ) for both IPC and TPC cases and several configurations<sup>7</sup>. Some important considerations are expressed hereinafter:

- From inspection of Fig. 2, it is apparent that both in IPC and TPC cases the ROC *can not be driven* toward the point  $(P_{D_0}, P_{F_0}) = (1, 0)$  merely increasing the number of sensors  $K$ , as long as the number of antennas  $N$  is kept finite, thus leading to zero (Bayesian and Neyman-Pearson) error-exponents [22]. Such results are analogous to the case of non-coherent DF with energy detection over diversity MAC [7].
- It is worth noticing that  $\bar{\Phi}_{-\tilde{\Lambda}}^I(s|\mathcal{H}_i)$  does not depend on  $\text{SNR}_*$ , as opposed to  $\bar{\Phi}_{-\tilde{\Lambda}}^T(s|\mathcal{H}_1)$  (which depends on  $\text{SNR}$ ); such difference is explained since, whichever  $(\text{SNR})_* < +\infty$  is assumed, we have that  $\text{SNR} \rightarrow +\infty$  in a large-system regime ( $K \rightarrow +\infty$ ).
- It can be verified that, when  $(P_D, P_F) = (1, 0)$ , Eqs. (22) and (23) reduce to  $\bar{\Phi}_{-\tilde{\Lambda}}^I(s|\mathcal{H}_1) = (1-s)^{-N}$  and  $\bar{\Phi}_{-\tilde{\Lambda}}^I(s|\mathcal{H}_0) = (1+s)^{-N}$ , respectively. In this case  $\tilde{\Lambda}^I|\mathcal{H}_1 \sim \Gamma(N; 1)$  and  $-\tilde{\Lambda}^I|\mathcal{H}_0 \sim \Gamma(N; 1)$ , thus leading to *ideal performance*<sup>8</sup> (i.e. the point  $(P_{D_0}, P_{F_0}) = (1, 0)$  belongs to the ROC). This is confirmed by observing that when  $(P_D, P_F) = (1, 0)$  Eq. (1) reduces to  $\mathbf{y} =$

<sup>7</sup>Note that looking at the figure, the concavity of the ROCs is not apparent, as instead suggested from the theory [15]; this is motivated by the use (throughout the paper) of a log-linear scale in the plot.

<sup>8</sup>Note that  $p_{-\tilde{\Lambda}}^I(\lambda|\mathcal{H}_1) \neq 0$ ,  $\lambda \in \mathbb{R}^+$ , and  $p_{-\tilde{\Lambda}}^I(\lambda|\mathcal{H}_0) \neq 0$ ,  $\lambda \in \mathbb{R}^-$ , i.e. the supports of the two pdfs are non-overlapping.

$(\mathbf{H}\mathbf{1}_K) \cdot \kappa + \mathbf{w}$ ,  $\kappa \in \{-1, 1\}$ ; in this case  $\Lambda_{MRC}$  represents the output of a standard MIMO-MRC combiner without beamforming [23] and the limit  $K \rightarrow +\infty$  under IPC determines  $\text{SNR} \rightarrow +\infty$  at the combiner. This consideration underlines the significant difference in terms of performance of the MRC in the context of DF (where  $(P_D, P_F) \neq (1, 0)$ ) w.r.t. its use in classic combining systems (where  $(P_D, P_F) = (1, 0)$ ).

- The large system ROC in both IPC and TPC cases can be driven toward the point  $(P_{D_0}, P_{F_0}) = (1, 0)$  by increasing also  $N$ . Such a result agrees with Eq. (13), where on the other hand  $K$  is kept finite and a large antenna array ( $N \rightarrow +\infty$ ) is considered. In fact, in the latter case the dependence on the specific channel realization vanishes, i.e. both the IC and the CA cases coincide, and MRC performance approaches those of a noisy counting rule, whose performance improves with  $K$ .

#### D. Area under the ROC

The AUC has been widely used as a global and synthetic measure of performance in machine learning applications [24]. Recently, it has been successfully applied to the performance analysis of communication systems employing diversity techniques [25], [26]. More specifically, in [25] the AUC has been derived in closed form and used for a theoretical comparison of several diversity combining statistics in the classic communication framework. In the case of non-coherent combining, an efficient formula for the AUC of energy detection, based on the MGF and Cauchy's theorem, has been recently proposed in [26].

The AUC is defined on the basis of Eqs. (14) and (15) as follows:

$$\text{AUC} \triangleq \int_0^1 P_{D_0}(\gamma) dP_{F_0}(\gamma) = - \int_{-\infty}^{+\infty} P_{D_0}(\gamma) \frac{\partial P_{F_0}(\gamma)}{\partial \gamma} d\gamma. \quad (26)$$

Note that, given the definition in Eq. (26),  $\text{AUC} \in [\frac{1}{2}, 1]$ , i.e. the performances of any fusion rule that exploits the measurements in a productive way cannot be worse than a strategy based on *flipping an unbiased coin*. The information given by the AUC can be alternatively expressed in terms of the *Gini index*, denoted as  $G_1$ , which is directly related to the AUC as follows [27]:

$$G_1 \triangleq 2 \cdot \text{AUC} - 1 \quad G_1 \in [0, 1]. \quad (27)$$

Note that in our case the AUC depends on the local sensor performance (i.e.  $P(\ell(\mathbf{x})|\mathcal{H}_i)$ ,  $\mathcal{H}_i \in \mathcal{H}$ ), the SNR, the number of sensors  $K$  and the number of antennas  $N$ . Unfortunately, the evaluation of the AUC of a detection statistic, through MC simulations, suffers from high computational complexity. In the following proposition we derive an alternative expression for the AUC which allows its efficient GC-based computation, similarly as shown for  $P_{D_0}(\gamma)$  and  $P_{F_0}(\gamma)$ .

**Proposition 4.** *The AUC in Eq. (26) can be expressed in the alternative form*

$$\text{AUC} = \int_{c-j\infty}^{c+j\infty} \frac{\Phi_{-\Lambda}(s|\mathcal{H}_1)\Phi_{-\Lambda}(-s|\mathcal{H}_0)}{2\pi j} \frac{ds}{s}. \quad (28)$$

where  $c$  is a positive constant in the RC of  $\Phi_{-\Lambda}(s|\mathcal{H}_1)$ .

*Proof:* The proof is given in Appendix D. ■

Eq. (26) is similar to the alternative expression derived in [28]; however the difference here is that Eq. (26) is not formulated in terms of a contour integral, which would require the evaluation of the residues of  $\frac{\Phi_{-\Lambda}(s|\mathcal{H}_1)\Phi_{-\Lambda}(-s|\mathcal{H}_0)}{s}$ , through the *Cauchy's theorem*. Differently, the AUC in Eq. (26) can be computed exploiting the GC quadrature rules, analogously as in Eqs. (17) and (18), through:

$$\text{AUC} \approx \frac{1}{\nu} \sum_{r=1}^{\nu/2} [\Re\{\psi(r)\} + \tau_r \Im\{\psi(r)\}]; \quad (29)$$

$$\psi(r) \triangleq \Phi_{-\Lambda}(\mu_r|\mathcal{H}_1)\Phi_{-\Lambda}(-\mu_r|\mathcal{H}_0); \quad (30)$$

where  $\nu$ ,  $\tau_r$  and  $\mu_r$  have the same meaning as in Eqs. (17) and (18).

#### V. SYSTEM DESIGN VIA DEFLECTION COEFFICIENTS

We have shown in Section IV that efficient computation of  $P_{F_0}(\gamma)$  and  $P_{D_0}(\gamma)$  can be obtained through Eqs. (16), (20) and (21). Also, the AUC, which represents a compact indicator for performance evaluation, can be evaluated through Eqs. (29) and (30) at low computational complexity. However, a compact and explicit metric (i.e. independent on  $\gamma$ , as the AUC, and available in closed form), suitable for system design, would be desirable. The deflection coefficient  $D_0$  and its modified version  $D_1$  are parameters<sup>9</sup> commonly employed in system design and analysis [14], while requiring only the first two order conditional moments. They are defined as follows [1], [14], [29]:

$$D_i \triangleq \frac{[\mathbb{E}\{\Lambda|\mathcal{H}_1\} - \mathbb{E}\{\Lambda|\mathcal{H}_0\}]^2}{\text{var}\{\Lambda|\mathcal{H}_i\}}, \quad i \in \{0, 1\}. \quad (31)$$

The expressions of  $\mathbb{E}\{\Lambda_{MRC}|\mathcal{H}_i\}$  and  $\text{var}\{\Lambda_{MRC}|\mathcal{H}_i\}$  are given in closed form by the following proposition.<sup>10</sup>

**Proposition 5.** *The mean and the variance of  $\Lambda_{MRC}|\mathcal{H}_i$  are:*

$$\mathbb{E}\{\Lambda_{MRC}|\mathcal{H}_i\} = 2N \mathbb{E}\{\ell|\mathcal{H}_i\} - KN; \quad (32)$$

$$\text{var}\{\Lambda_{MRC}|\mathcal{H}_i\} = K^2N \left(1 + \frac{1}{2\text{SNR}}\right) - 2KN \mathbb{E}\{\ell|\mathcal{H}_i\} + 2N \mathbb{E}\{\ell^2|\mathcal{H}_i\} + 4N^2 \text{var}\{\ell|\mathcal{H}_i\}. \quad (33)$$

*Proof:* The moments of  $\Lambda_{MRC}|\mathcal{H}_i$  are evaluated through the MGF definition [30]:

$$\mathbb{E}\{(\Lambda_{MRC})^m|\mathcal{H}_i\} = \left. \frac{d^m [\Phi_{-\Lambda_{MRC}}(s|\mathcal{H}_i)]}{ds^m} \right|_{s=0} \quad (34)$$

<sup>9</sup>In the specific case of a mean-shifted Gauss-Gauss hypothesis testing, they coincide and represent the SNR of the statistic under Neyman-Pearson framework [15].

<sup>10</sup>Hereinafter, we drop the dependence of  $\ell(\cdot)$  w.r.t.  $\mathbf{x}$  for ease of notation.

Hence, the first two order moments are obtained by setting  $m = 1$  and  $m = 2$ , respectively. Finally, the variance is computed as  $\text{var}\{\Lambda_{MRC}|\mathcal{H}_i\} = \mathbb{E}\{\Lambda_{MRC}^2|\mathcal{H}_i\} - \mathbb{E}\{\Lambda_{MRC}|\mathcal{H}_i\}^2$ . ■

As a corollary we also report  $D_i^{MRC}$  explicitly in the case of conditionally i.i.d. sensor decisions.

**Corollary 1.** *The deflection coefficients, when  $P(\mathbf{x}|\mathcal{H}_i) = \prod_{k=1}^K P(x_k|\mathcal{H}_i)$ ,  $\mathcal{H}_i \in \mathcal{H}$ , and  $(P_{D,k}, P_{F,k}) = (P_D, P_F)$ ,  $k \in \mathcal{K}$ , are given by:*

$$D_i^{MRC} = \frac{4NK(P_D - P_F)^2}{K(1 + \frac{1}{2\text{SNR}}) + 2(2N + 1 - K)\rho_i}, \quad i \in \{0, 1\}, \quad (35)$$

where  $\rho_0 \triangleq P_F(1 - P_F)$  and  $\rho_1 \triangleq P_D(1 - P_D)$ .

We will now analyze the qualitative behaviour of the deflection coefficients (we will restrict our attention, for sake of simplicity, to  $D_i^{MRC}$  in the conditionally i.i.d. case) in order to assess their efficacy (in this specific problem) for analysis and design purposes. In fact it is worth remarking that, as carefully specified in [14], an *improvement in the deflection coefficients* in a generic detection problem *does not guarantee a corresponding improvement in terms of  $\{P_{F_0}, P_{D_0}\}$*  and thus they should be used with care.

We start noticing that  $D_i^{MRC}$  is strictly increasing with  $K$  under both IPC and TPC cases. Therefore, the large-system (i.e.  $K \rightarrow +\infty$ ) deflections

$$\bar{D}_i^{MRC,I} = \frac{4N(P_D - P_F)^2}{1 - 2\rho_i}, \quad (36)$$

$$\bar{D}_i^{MRC,T} = \frac{4N(P_D - P_F)^2}{(1 + \frac{1}{2\text{SNR}}) - 2\rho_i}, \quad i \in \{0, 1\}, \quad (37)$$

represent the maximum attainable, when  $N$  (and SNR under TPC) is kept fixed. Some important observations are listed hereinafter:

- From inspection of Eqs. (36) and (37), we have that  $\bar{D}_i^{MRC,T} < \bar{D}_i^{MRC,I} < +\infty$ , i.e. the large-system deflection coefficients under both IPC and TPC are finite, thus being in agreement with non-ideal performance shown in Subsection IV-C.
- As  $\text{SNR} \rightarrow +\infty$  in Eq. (37), we have  $\bar{D}_i^{MRC,T} \rightarrow \bar{D}_i^{MRC,I}$ , thus being in agreement with Fig. 2 where CA-ROC under TPC approaches that under IPC as SNR increases.
- Taking  $N \rightarrow +\infty$  in Eqs. (36) and (37) we get  $\bar{D}_i^{MRC,I} = \bar{D}_i^{MRC,T} = +\infty$ ; this result agrees with the ideal performance attainable in a large-system regime when we let  $N$  grow (cf. Fig. 2).
- If we set  $(P_D, P_F) = (1, 0)$  (i.e. the perfect sensor assumption) in Eq. (36) we obtain  $\bar{D}_i^{MRC,I} = 4N$ ; this *disagrees with the ideal performance* attained in a large-system regime under IPC (see second bullet in Subsection IV-C). Such discrepancy is explained since, under the aforementioned assumptions, we have  $\tilde{\Lambda}^I|\mathcal{H}_1 \xrightarrow{d} \Gamma(N; 1)$  and  $-\tilde{\Lambda}^I|\mathcal{H}_0 \xrightarrow{d} \Gamma(N; 1)$ , i.e. the pdfs  $p_{\tilde{\Lambda}^I}(\lambda|\mathcal{H}_0)$  and

$p_{\tilde{\Lambda}^I}(\lambda|\mathcal{H}_1)$  have a *non-zero variance but non-overlapping supports*<sup>11</sup>.

On the basis of the previous considerations it can be deduced that  $D_i^{MRC}$ ,  $i \in \{0, 1\}$ , cannot be effectively used for performance analysis of MRC, but that it can be rather suited for system design, since it retains the same dependence on the WSN parameters as the CA-ROC. For this reason we will use the (modified) deflection as an optimization metric in order to obtain a choice of the sensor threshold. We will formulate here the optimization w.r.t.  $P_F$ , since we make the reasonable assumption that a *one-to-one* mapping between the local threshold and  $P_F$  exists. More specifically, exploiting Eq. (35), we are interested in obtaining:

$$P_F^{*,i} \triangleq \arg \max_{P_F} D_i^{MRC}(P_F) \quad (38)$$

$$= \arg \max_{P_F} \frac{4NK \cdot (P_D(P_F) - P_F)^2}{K(1 + \frac{1}{2\text{SNR}}) + 2 \cdot (2N + 1 - K) \cdot \rho_i(P_F)}. \quad (39)$$

It can be noticed that  $D_i^{MRC}(P_F)$ , as it will be shown in Section VI through simulations, is *quasi-concave* (i.e. unimodal) [31]. Thus local-optimization procedures, based on standard *quasi-convex programming*, can be easily devised in order to obtain  $P_F^{*,i}$ . However, the derivation and comparison of such procedures is outside the scope of this work. The improvement in terms of performance on the CA-ROC, attained with such optimization, will be verified in Section VI.

## VI. NUMERICAL RESULTS

In this section we verify and analyze the theoretical results obtained in Sections IV and V. For simplicity and w.l.o.g. we consider conditionally i.i.d. sensor decisions, i.e.  $P(\mathbf{x}|\mathcal{H}_i) = \prod_{k=1}^K P(x_k|\mathcal{H}_i)$ ,  $\mathcal{H}_i \in \mathcal{H}$ , and  $(P_{D,k}, P_{F,k}) = (P_D, P_F)$ ,  $k \in \mathcal{K}$ . Unless differently stated, we assume  $(P_D, P_F) \triangleq (0.5, 0.05)$ , as adopted in [1], [3] for fusion rules comparison over PAC.

*IC false-alarm rate with threshold  $\check{\gamma}$* : In Fig. 3 we assess the accuracy of  $\check{\gamma}$  (given by Eq. (10)) through MC simulations; we choose here  $\check{P}_{F_0} = 0.01$ . The experiment is conducted as follows. We generate  $(2 \cdot 10^3)$  realizations of  $\mathbf{H}$  and, for each of these, we generate  $10^4$  realizations of  $(\mathbf{w}, \mathbf{x})$  to obtain an estimate of  $P_{F_0}(\check{\gamma}, \mathbf{H})$ . Finally an histogram of the r.v.  $P_{F_0}(\check{\gamma}, \mathbf{H})$  is obtained by considering all the realizations of  $\mathbf{H}$ . We report the cases corresponding to  $N \in \{1, 2\}$ ,  $(\text{SNR})_{dB} \in \{-5, 0\}$  and  $K \in \{50, 100\}$ . Since  $\check{\gamma}$  is a low-SNR and large-system approximation, as the SNR decreases and  $K$  increases the histogram approaches a delta function centered at the desired IC false-alarm rate; furthermore it can be seen that a low-SNR assures unbiasedness of the estimate, while increasing  $K$  reduces the variance of the histogram.

*MC vs GC rules CA-ROC*: Fig. 4 shows the CA-ROC of the MRC rule in a WSN with  $K = 8$  and  $N = 2$  at the DFC in two scenarios with different  $P_D$  (we fix  $P_F = 0.05$ ): (a)  $P_D = 0.5$ ; (b)  $P_D = 0.7$ . For sake of completeness

<sup>11</sup>In fact, it can be easily verified that when  $K \rightarrow +\infty$  and  $(P_D, P_F) = (1, 0)$ , we have  $E\{\tilde{\Lambda}^I|\mathcal{H}_1\} = N$ ,  $E\{\tilde{\Lambda}^I|\mathcal{H}_0\} = -N$  and  $\text{var}\{\tilde{\Lambda}^I|\mathcal{H}_i\} = N$ .

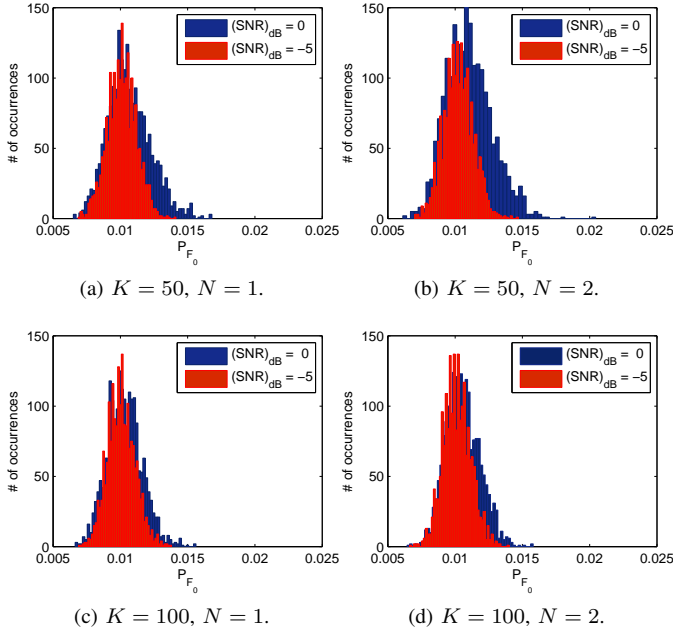


Figure 3: Threshold choice  $\check{\gamma}$  for target  $\check{P}_{F_0} = 0.01$ ;  $(P_{D,k}, P_{F,k}) = (0.5, 0.05)$ ,  $k \in \mathcal{K}$ .

we also report the CA-ROC of Max-Log fusion rule (in dashed lines), which represents an approximated and efficient implementation of the optimum in Eq. (3), but exhibiting negligible performance loss [13]. For each scenario we report the performance at  $(\text{SNR})_{dB} \in \{5, 10, 15\}$ . Solid lines represent GC-based computation of MRC CA-ROC ( $\nu = 10^3$  for each value of  $\gamma$ ), while square markers represent the corresponding MC-based evaluation ( $10^5$  runs for each value of  $\gamma$ ), in the two scenarios respectively. It is apparent how the proposed approach perfectly matches the MC simulations, while requiring dramatically reduced computational resources (the complexity is in fact reduced *roughly by two orders of magnitude*<sup>12</sup>). Finally, it is also apparent the increasing performance loss of MRC with respect to Max-Log as the SNR increases (since MRC is a low-SNR approximation of the optimum rule).

$P_{D_0}$  vs  $K$ : In Fig. 5 we report  $P_{D_0}$  as a function of the number of sensors  $K$ , under  $P_{F_0} = 0.01$ ; we show the performance for several configurations of  $(\text{SNR})_{dB}$  under TPC (resp.  $(\text{SNR}_*)_{dB}$  under IPC) and  $N$ . Firstly, the figure confirms that GC-based computation ( $\nu = 10^3$  for each value of  $\gamma$  of each considered CA-ROC, plotted with solid lines) perfectly matches the MC simulations ( $10^5$  runs for each value of  $\gamma$  of each considered CA-ROC, plotted with plus markers). Secondly, as  $K$  increases, there is a saturation effect in  $P_{D_0}$ , which converges to a value smaller than 1. Such a result is perfectly predicted through GC-based computation ( $\nu = 10^3$  for each value of  $\gamma$  of each considered CA-ROC, plotted in

<sup>12</sup>Even if the two approaches are not directly comparable, we observe that in the former case the complexity is proportional to  $\nu$ , while with MC-based computation it is proportional to the number of runs. Furthermore, when using the GC-based computation,  $\nu$  could be further reduced through an optimized choice of  $c$ .

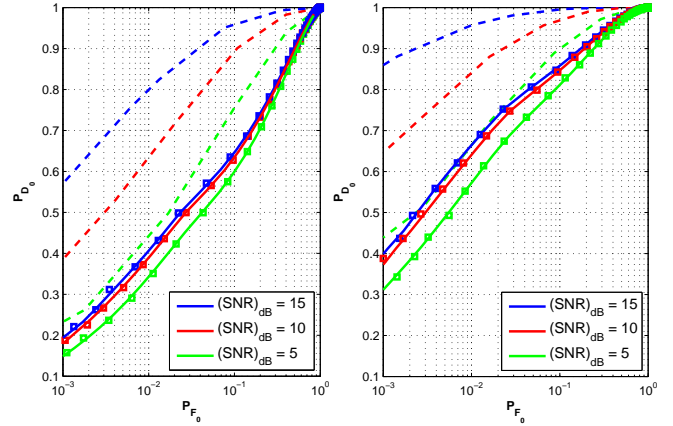


Figure 4: Max-Log (dashed lines), GC-based MRC (solid lines) and MC-based MRC ( $\square$  markers) CA-ROC evaluation. WSN with  $K = 8$ ,  $N = 2$ ,  $(\text{SNR})_{dB} \in \{5, 10, 15\}$ .  $(P_{D,k}, P_{F,k}) = (0.5, 0.05)$  for scenario (a) (left plot),  $(P_{D,k}, P_{F,k}) = (0.7, 0.05)$  for scenario (b) (right plot),  $k \in \mathcal{K}$ .

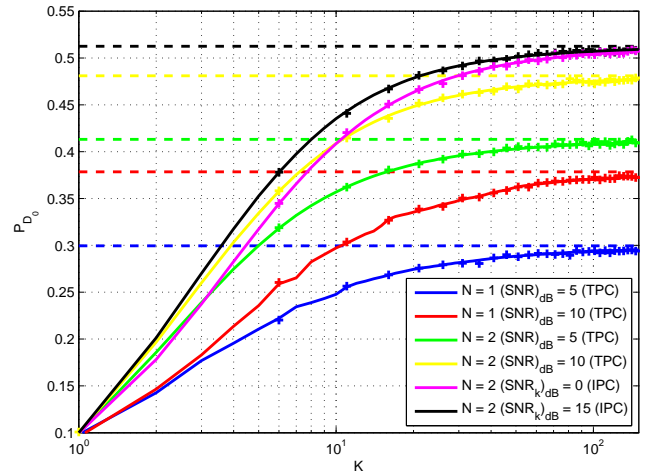


Figure 5:  $P_{D_0}$  vs  $K$ ,  $P_{F_0} = 0.01$ ;  $(P_{D,k}, P_{F,k}) = (0.5, 0.05)$ ,  $k \in \mathcal{K}$ . Solid lines denote GC-based  $P_{D_0}$ , while plus (+) markers refer to MC-based  $P_{D_0}$ ; finally dotted lines denote GC-based  $P_{D_0}$  evaluation through large-system conditional MGFs.

dotted lines) of large-system conditional MGFs in Eqs. (22-25), thus confirming Proposition 3. Finally, we remark that a similar behaviour has been observed when considering the overall CA-ROC performance, expressed in terms of  $G_1$ .

$G_1$  vs  $(K, N)$ : In Fig. 6 we illustrate  $G_1$  as a function of both  $K$  and  $N$  to investigate how performance saturation can be avoided. We consider both IPC ( $(\text{SNR}_*)_{dB} = 10$ ) and TPC ( $(\text{SNR})_{dB} = 10$ ), in Figs. 6a and 6b, respectively; it is worth remarking that similar behaviours have been observed for different values of  $(\text{SNR})_{dB}$  and  $(\text{SNR}_*)_{dB}$ . Each surface is obtained exploiting GC-based computation (only  $\nu = 64$ ) in Eqs. (29) and (30); the corresponding MC-based  $G_1$  is not reported for sake of clarity, since a *perfect match has been noticed*. The surfaces show that when either  $K$  or  $N$  is kept fixed and the other parameter grows we cannot attain



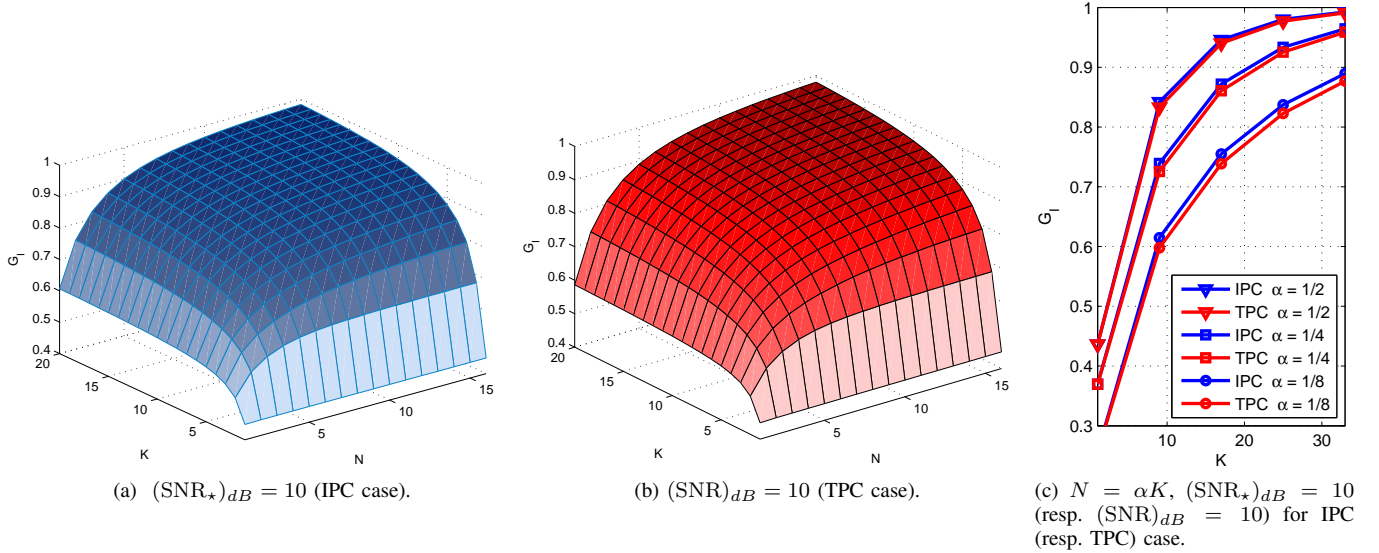


Figure 6:  $G_1$  vs  $(K, N)$ ;  $(P_{D,k}, P_{F,k}) = (0.5, 0.05)$ ,  $k \in \mathcal{K}$ .

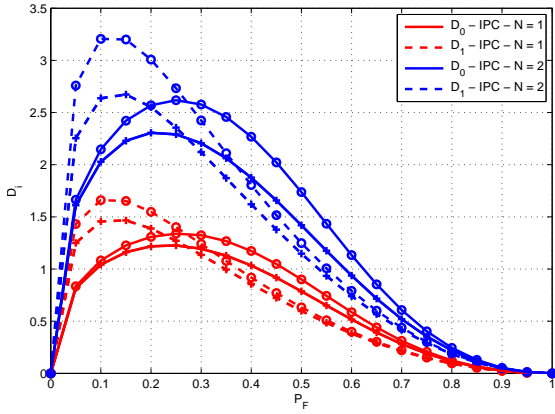
$G_1 = 1$  (i.e. ideal performance) both in IPC and TPC cases. Differently, we observe that ideal performances are achievable when both the parameters increase simultaneously. For this reason, in Fig. 6c we analyze  $G_1$  after fixing  $N = \alpha K$  (we consider  $\alpha \in \{\frac{1}{2}, \frac{1}{4}, \frac{1}{8}\}$ , since it is reasonable to assume that typically  $K > N$ ) and let  $K$  grow. It is apparent that in this setup: (i) we can achieve ideal performance as  $K$  increases; (ii) the value of  $K$  needed to achieve ideal performance decreases as  $\alpha \rightarrow 1$ ; (iii) the performance of IPC and TPC cases are roughly the same as  $K$  grows, since increasing  $N$  corresponds to an increase of the received SNR, *independently* on the specific power constraint assumed.

*Sensor threshold optimization via  $D_i^{MRC}$* : In Fig. 7 we illustrate the effect of a  $D_i^{MRC}$ -optimized choice for  $P_F$ . We consider the scenarios  $K \in \{15, 50\}$  and  $(\text{SNR})_{dB} = 5$  under TPC (resp.  $(\text{SNR}_*)_{dB} = 5$  under IPC). We assume that the generic sensor is a detector of a *change-in-variance* [15], whose closed-form expression is given by  $P_D(P_F) = P_F^{1/(1+\text{SNR}_{obs})}$ , where  $\text{SNR}_{obs}$  denotes *sensing* SNR; we choose  $(\text{SNR}_{obs})_{dB} = 5$ . We compare the performance when: (i)  $P_F = 0.05$  (non-optimized choice); (ii)  $P_F = P_F^{*,1}$  (i.e.  $D_1^{MRC}$ -optimized, recall Eq. (39)); (iii)  $P_F = P_F^{*,0}$  (i.e.  $D_0^{MRC}$ -optimized, recall Eq. (39)). In Figs. 7a and 7c we show the corresponding  $D_i^{MRC}(P_F)$  under IPC and TPC, respectively, for all the scenarios considered ( $D_0^{MRC}$  and  $D_1^{MRC}$  in solid and dotted lines, respectively;  $K = 15$  and  $K = 50$  with plus and circle markers, respectively); all the curves underline *quasi-concavity* of  $D_i^{MRC}(P_F)$ . In Figs. 7b and 7d we show  $P_{D_0}$  (GC-based computation,  $\nu = 10^3$  for each value of  $\gamma$  of each considered CA-ROC) as a function of the number of antennas  $N$ , under  $P_{F_0} = 0.01$ , in IPC and TPC case, respectively. First, it is apparent that deflection-based optimization of  $P_F$  becomes effective, in comparison to a non-optimized choice, as  $N$  grows. Furthermore, the improvement is more pronounced in the case  $K = 50$  where the choice becomes effective for small  $N$  (i.e.  $N > 2$

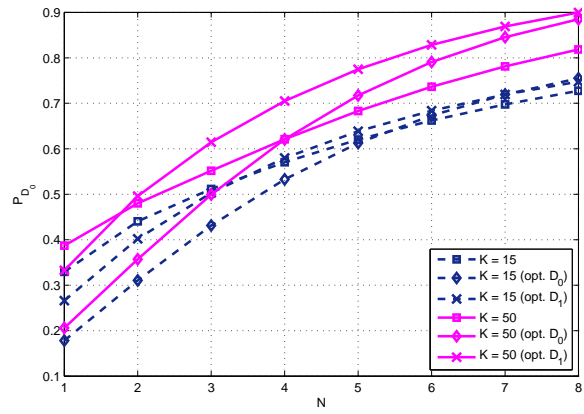
when  $P_F = P_F^{*,1}$ ); therefore such threshold optimization is *best-suited* for a large-system. For example, when choosing  $P_F = P_F^{*,1}$ , a 10% improvement of  $P_{D_0}$  is achieved in a configuration with  $(K, N) = (50, 4)$ . Also, it is observed that the choice  $P_F = P_F^{*,1}$  is more convenient w.r.t.  $P_F = P_F^{*,0}$  for this setup; this is due to the higher detection sensitivity ensured when optimizing  $P_F$  w.r.t.  $D_1^{MRC}$ , in a Neyman-Pearson scenario (i.e. a fixed  $P_{F_0}$ ). Finally, it is worth noticing that performance improvement effect is similar under both IPC and TPC.

## VII. CONCLUSIONS

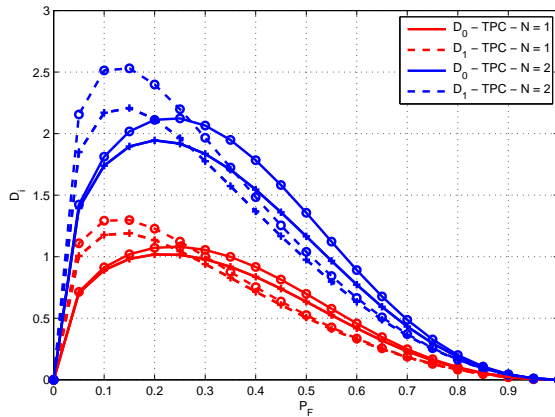
In this paper we presented a performance analysis of MRC DF rule over MIMO channels. We derived an approximate threshold choice with reduced requirements on system knowledge, useful at low-SNR and in a large-system regime, exploiting IC probabilities of false alarm and detection. Also, the CA conditional MGF was derived in closed form in order to compute efficiently the CA system probabilities of false alarm and detection via GC rules. The explicit expression of CA conditional MGFs was also exploited to demonstrate that ideal performance is not attained in large-system limit under both IPC and TPC. The CA conditional MGF was also used to derive an efficient computation of the AUC of the proposed statistic, which was shown to be suited for synthetic performance analysis w.r.t the WSN parameters. The AUC analysis also showed how performance saturation can be avoided by increasing accordingly the number of sensors and antennas. Finally, the (modified) deflection coefficient was derived in closed form and it was shown to be effective as an optimization metric for the local threshold choice, when the DFC has multiple antennas. Such effect was shown to be more pronounced when the number of sensors is large.



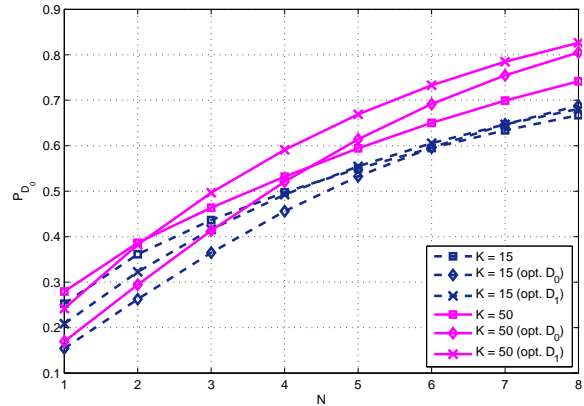
(a)  $D_i^{MRC}$  vs  $P_F$ ; IPC case,  $(\text{SNR}_*)_{dB} = 5$ . Plus (+) and circle (o) markers refer to  $K = 15$  and  $K = 50$ , respectively.



(b)  $P_{D_0}$  vs  $N$ ;  $P_{F_0} = 0.01$ . WSN with  $K \in \{15, 50\}$ ; IPC case,  $(\text{SNR}_*)_{dB} = 5$ . Square (+) markers refer to  $P_F = 0.05$  (non-optimized), diamonds ( $\diamond$ ) to  $P_F = P_F^{*,0}$  and cross markers ( $\times$ ) to  $P_F = P_F^{*,1}$ .



(c)  $D_i^{MRC}$  vs  $P_F$ ; TPC case,  $(\text{SNR})_{dB} = 5$ . Plus (+) and circle (o) markers refer to  $K = 15$  and  $K = 50$ , respectively.



(d)  $P_{D_0}$  vs  $N$ ;  $P_{F_0} = 0.01$ . WSN with  $K \in \{15, 50\}$ ; TPC case,  $(\text{SNR})_{dB} = 5$ . Square (+) markers refer to  $P_F = 0.05$  (non-optimized), diamonds ( $\diamond$ ) to  $P_F = P_F^{*,0}$  and cross markers ( $\times$ ) to  $P_F = P_F^{*,1}$ .

Figure 7: Performance comparison of  $D_i^{MRC}$ -optimized vs non-optimized  $P_F$  for MRC.  $(\text{SNR}_{obs})_{dB} = 5$ .

## VIII. ACKNOWLEDGEMENTS

The authors would like to express their sincere gratitude to the Associate Editor and the anonymous reviewers for taking their time into reviewing this manuscript and providing comments that contributed to improve the quality and the readability of the manuscript.

### APPENDIX A PROOF OF PROPOSITION 1

In the first part of this Appendix we will derive the closed form expression for  $p_{\Lambda_{MRC}}(\lambda|\mathbf{H}, \mathcal{H}_i)$ ,  $\lambda \in \mathbb{R}$ ,  $\mathcal{H}_i \in \mathcal{H}$ . From inspection of Eqs. (3) and (4) it can be shown that, since the pdf of  $\mathbf{y}|\mathbf{H}, \mathcal{H}_i$  is a Gaussian mixture with weights equal to  $P(\mathcal{H}_i)$ , also  $\Lambda_{MRC}|\mathbf{H}, \mathcal{H}_i$  will be distributed according to a Gaussian mixture with the same weights (as the MRC rule represents a widely-linear transformation of  $\mathbf{y}$  [32]), that is

$$\Lambda_{MRC}|\mathbf{H}, \mathcal{H}_i \sim \quad (40)$$

$$\sum_{\mathbf{x} \in \mathcal{X}^K} P(\mathbf{x}|\mathcal{H}_i) \mathcal{N}(E\{\Lambda_{MRC}|\mathbf{H}, \mathbf{x}\}, \text{var}\{\Lambda_{MRC}|\mathbf{H}, \mathbf{x}\}).$$

To obtain a complete characterization of Eq. (40) we now evaluate the mean and the variance of each component of the mixture; for this purpose let us define  $\tilde{\mathbf{z}}_{MRC} \triangleq \frac{1}{2} [ \mathbf{z}_{MRC}^t \quad \mathbf{z}_{MRC}^\dagger ]^t$ ,  $\tilde{\mathbf{H}} \triangleq [ \mathbf{H}^t \quad \mathbf{H}^\dagger ]^t$ ,  $\tilde{\mathbf{y}} \triangleq [ \mathbf{y}^t \quad \mathbf{y}^\dagger ]^t$  and  $\tilde{\mathbf{w}} \triangleq [ \mathbf{w}^t \quad \mathbf{w}^\dagger ]^t$ . The mean of  $\Lambda_{MRC}|\mathbf{H}, \mathbf{x}$  is obtained as follows

$$\mathbb{E}\{\Lambda_{MRC}|\mathbf{H}, \mathbf{x}\} = \mathbb{E}\{\tilde{\mathbf{z}}_{MRC}^\dagger \tilde{\mathbf{y}}|\mathbf{H}, \mathbf{x}\} \quad (41)$$

$$= \tilde{\mathbf{z}}_{MRC}^\dagger \tilde{\mathbf{H}} \mathbf{x} \quad (42)$$

$$= \Re(\tilde{\mathbf{z}}_{MRC}^\dagger \mathbf{H} \mathbf{x}), \quad (43)$$

where we exploited  $\tilde{\mathbf{y}} = \tilde{\mathbf{H}}\mathbf{x} + \tilde{\mathbf{w}}$  and  $\mathbb{E}\{\tilde{\mathbf{w}}\} = \mathbf{0}_{2N}$ . Differently, the variance is evaluated as

$$\text{var}\{\Lambda_{MRC}|\mathbf{H}, \mathbf{x}\} = \mathbb{E}\left\{\left\|\tilde{\mathbf{z}}_{MRC}^\dagger \tilde{\mathbf{y}} - \tilde{\mathbf{z}}_{MRC}^\dagger \tilde{\mathbf{H}}\mathbf{x}\right\|^2|\mathbf{H}, \mathbf{x}\right\} \quad (44)$$

$$= \mathbb{E}\left\{\left\|\tilde{\mathbf{z}}_{MRC}^\dagger \tilde{\mathbf{w}}\right\|^2|\mathbf{H}\right\} \quad (45)$$

$$= \tilde{\mathbf{z}}_{MRC}^\dagger \mathbb{E}\{\tilde{\mathbf{w}}\tilde{\mathbf{w}}^\dagger\} \tilde{\mathbf{z}}_{MRC} \quad (46)$$

$$= \frac{\sigma_w^2}{2} \|\mathbf{z}_{MRC}\|^2 \quad (47)$$

since  $\mathbf{w}$  is independent on both  $\mathbf{H}$  and  $\mathbf{x}$  and  $\mathbb{E}\{\tilde{\mathbf{w}}\tilde{\mathbf{w}}^\dagger\} = \sigma_w^2 \mathbf{I}_{2N}$ . Direct substitution of Eqs. (43) and (47) in Eq. (40) provides Eq. (7).

We will now prove Proposition 1. We start noticing that at low-SNR the components of the mixture will be concentrated and thus we can rely on the *Gaussian moment matching* [33] to approximate the pdf in Eq. (40) as

$$\Lambda_{MRC}|\mathbf{H}, \mathcal{H}_i \stackrel{\text{approx.}}{\sim} \mathcal{N}(\mathbb{E}\{\Lambda_{MRC}|\mathbf{H}, \mathcal{H}_i\}, \text{var}\{\Lambda_{MRC}|\mathbf{H}, \mathcal{H}_i\}). \quad (48)$$

To accomplish this task we need to evaluate the mean and variance of  $\Lambda_{MRC}|\mathbf{H}, \mathcal{H}_i$ . The mean is obtained as

$$\mathbb{E}\{\Lambda_{MRC}|\mathbf{H}, \mathcal{H}_i\} = \sum_{\mathbf{x} \in \mathcal{X}^K} \mathbb{E}\{\Lambda_{MRC}|\mathbf{H}, \mathbf{x}\} P(\mathbf{x}|\mathcal{H}_i) \quad (49)$$

$$= \sum_{\mathbf{x} \in \mathcal{X}^K} \Re\{\mathbf{z}_{MRC}^\dagger \mathbf{H}\mathbf{x}\} P(\mathbf{x}|\mathcal{H}_i) \quad (50)$$

$$= \Re\{\mathbf{z}_{MRC}^\dagger \mathbf{H}\mathbb{E}\{\mathbf{x}|\mathcal{H}_i\}\} \quad (51)$$

where we exploited the explicit expression of  $\mathbb{E}\{\Lambda_{MRC}|\mathbf{H}, \mathbf{x}\}$  in Eq. (43). Differently, the variance is obtained as

$$\begin{aligned} \text{var}\{\Lambda_{MRC}|\mathbf{H}, \mathcal{H}_i\} &= \\ \sum_{\mathbf{x} \in \mathcal{X}^K} \mathbb{E}\left\{\left\|\Lambda_{MRC} - \tilde{\mathbf{z}}_{MRC}^\dagger \tilde{\mathbf{H}}\mathbb{E}\{\mathbf{x}|\mathcal{H}_i\}\right\|^2|\mathbf{H}, \mathbf{x}\right\} P(\mathbf{x}|\mathcal{H}_i) &= \end{aligned} \quad (52)$$

$$\sum_{\mathbf{x} \in \mathcal{X}^K} \mathbb{E}\left\{\left\|\tilde{\mathbf{z}}_{MRC}^\dagger \cdot \left(\tilde{\mathbf{y}} - \tilde{\mathbf{H}}\mathbb{E}\{\mathbf{x}|\mathcal{H}_i\}\right)\right\|^2|\mathbf{H}, \mathbf{x}\right\} P(\mathbf{x}|\mathcal{H}_i) = \quad (53)$$

$$\begin{aligned} \sum_{\mathbf{x} \in \mathcal{X}^K} \left(\mathbb{E}\left\{\left\|\tilde{\mathbf{z}}_{MRC}^\dagger \tilde{\mathbf{H}}(\mathbf{x} - \mathbb{E}\{\mathbf{x}|\mathcal{H}_i\})\right\|^2|\mathbf{H}, \mathbf{x}\right\} + \right. \\ \left. \mathbb{E}\left\{\left\|\tilde{\mathbf{z}}_{MRC}^\dagger \tilde{\mathbf{w}}\right\|^2|\mathbf{H}\right\}\right) P(\mathbf{x}|\mathcal{H}_i) = \end{aligned} \quad (54)$$

$$\tilde{\mathbf{z}}_{MRC}^\dagger \tilde{\mathbf{H}}\mathbf{C}(\mathbf{x}|\mathcal{H}_i) \tilde{\mathbf{H}}^\dagger \tilde{\mathbf{z}}_{MRC} + \frac{\sigma_w^2}{2} \|\mathbf{z}_{MRC}\|^2, \quad (55)$$

where  $\mathbf{C}(\mathbf{x}|\mathcal{H}_i) \triangleq \mathbb{E}\{(\mathbf{x} - \mathbb{E}\{\mathbf{x}|\mathcal{H}_i\})(\mathbf{x} - \mathbb{E}\{\mathbf{x}|\mathcal{H}_i\})^T|\mathcal{H}_i\}$ . Therefore, in view of these results and exploiting Eq. (48), we obtain the following low-SNR approximation for  $P_{F_0}(\mathbf{H})$ :

$$P_{F_0}(\mathbf{H}) \approx \mathcal{Q}\left(\frac{\gamma - \Re\{\mathbf{z}_{MRC}^\dagger \mathbf{H}\mathbb{E}\{\mathbf{x}|\mathcal{H}_0\}\}}{\sqrt{\tilde{\mathbf{z}}_{MRC}^\dagger \tilde{\mathbf{H}}\mathbf{C}(\mathbf{x}|\mathcal{H}_0) \tilde{\mathbf{H}}^\dagger \tilde{\mathbf{z}}_{MRC} + \frac{\sigma_w^2}{2} \|\mathbf{z}_{MRC}\|^2}}\right). \quad (56)$$

Under the simplifying assumptions  $\mathbb{E}\{\mathbf{x}|\mathcal{H}_0\} = (2P_F - 1)\mathbf{1}_K$  and  $\mathbf{C}(\mathbf{x}|\mathcal{H}_0) = [1 - (2P_F - 1)^2] \mathbf{I}_K$  (i.e. the threshold of each sensor is set to assure the same  $P_F$  and also the decisions are uncorrelated, given  $\mathcal{H}_0$ ), Eq. (56) simplifies to:

$$P_{F_0}(\mathbf{H}) \approx \mathcal{Q}\left(\frac{\gamma - \delta \cdot \|\mathbf{z}_{MRC}\|^2}{\sqrt{(1 - \delta^2) \cdot \tilde{\mathbf{z}}_{MRC}^\dagger \tilde{\mathbf{H}} \tilde{\mathbf{H}}^\dagger \tilde{\mathbf{z}}_{MRC} + \frac{\sigma_w^2}{2} \|\mathbf{z}_{MRC}\|^2}}\right), \quad (57)$$

where  $\delta \triangleq (2P_F - 1)$ . Eq. (57) still contains a problematic dependence w.r.t. the entire channel matrix  $\mathbf{H}$ ; therefore we consider a large-system ( $K \rightarrow +\infty$ ) regime, where  $\tilde{\mathbf{H}} \tilde{\mathbf{H}}^\dagger \approx 2K \mathbf{I}_N$  holds, thus leading to

$$P_{F_0}(\mathbf{H}) \approx \mathcal{Q}\left(\frac{\gamma - \delta \|\mathbf{z}_{MRC}\|^2}{\sqrt{\frac{1}{2}((1 - \delta^2) \cdot K + \sigma_w^2) \|\mathbf{z}_{MRC}\|^2}}\right), \quad (58)$$

which can be easily inverted to provide Eq. (10).

## APPENDIX B PROOF OF PROPOSITION 2

We derive here the closed form of  $\Phi_{-\Lambda_{MRC}}(s|\mathbf{x})$  in Eq. (20). Similarly to [34], where the symbol-error probability in a fading environment with antenna diversity was obtained, we express  $-\Lambda_{MRC}|\mathbf{x}$  as follows

$$-\Lambda_{MRC}|\mathbf{x} = \sum_{n=1}^N (\mathbf{v}_n|\mathbf{x})^\dagger \cdot \mathbf{F} \cdot (\mathbf{v}_n|\mathbf{x}), \quad (59)$$

where the Gaussian vectors  $(\mathbf{v}_n|\mathbf{x})$ ,  $n \in \{1, \dots, N\}$ , and the deterministic matrix  $\mathbf{F}$  have the explicit expressions:

$$\mathbf{v}_n|\mathbf{x} \triangleq [y_n|\mathbf{x} \quad \mathbf{h}_{r,n} \mathbf{1}_K]^\dagger \quad \mathbf{F} \triangleq \begin{bmatrix} 0 & -\frac{1}{2} \\ -\frac{1}{2} & 0 \end{bmatrix} \quad (60)$$

with  $\mathbf{h}_{r,n}$  denoting the  $n$ th row of  $\mathbf{H}$ . Note that Eq. (59) is a sum of Hermitian quadratic forms of circularly complex Gaussian vectors  $\mathbf{v}_n|\mathbf{x}$ . Since  $\mathbf{v}_n|\mathbf{x}$  are i.i.d. vectors, the Laplace transform of Eq. (59) has the following closed form [30]:

$$\Phi_{-\Lambda_{MRC}}(s|\mathbf{x}) = \left[\frac{1}{\det(\mathbf{I}_2 + s\mathbf{L}(\mathbf{x}))}\right]^N \quad (61)$$

where  $\mathbf{L}(\mathbf{x}) \triangleq (\mathbf{R}|\mathbf{x}) \cdot \mathbf{F}$  and  $\mathbf{R}|\mathbf{x} \triangleq \mathbb{E}\{(\mathbf{v}_n|\mathbf{x})(\mathbf{v}_n|\mathbf{x})^\dagger\}$ , i.e. the covariance matrix of  $\mathbf{v}_n|\mathbf{x}$ , since  $\mathbb{E}\{(\mathbf{v}_n|\mathbf{x})\} = \mathbf{0}_2$ . The explicit expression of  $\mathbf{R}|\mathbf{x}$  is:

$$\mathbf{R}|\mathbf{x} = \mathbb{E}\{(\mathbf{v}_n|\mathbf{x})(\mathbf{v}_n|\mathbf{x})^\dagger\} \quad (62)$$

$$= \begin{bmatrix} K + \sigma_w^2 & 2\ell(\mathbf{x}) - K \\ 2\ell(\mathbf{x}) - K & K \end{bmatrix}. \quad (63)$$

Denoting  $\lambda_i(\mathbf{x})$ ,  $i \in \{1, 2\}$ , the two eigenvalues of  $\mathbf{L}(\mathbf{x})$  we have that

$$\Phi_{-\Lambda_{MRC}}(s|\mathbf{x}) = \left[\frac{1}{(1 + s\lambda_1(\mathbf{x}))(1 + s\lambda_2(\mathbf{x}))}\right]^N. \quad (64)$$

Evaluation of  $\lambda_i(\mathbf{x})$ , through  $\det(s\mathbf{I}_2 - \mathbf{L}(\mathbf{x})) = 0$ , gives:

$$\lambda_i(\mathbf{x}) = \frac{1}{2} \cdot \left(K - 2\ell(\mathbf{x}) \pm K \sqrt{1 + \frac{1}{\text{SNR}}}\right), \quad (65)$$

where we have exploited that  $\text{SNR} = \frac{K}{\sigma_w^2}$ . Direct substitution of explicit expression of  $\lambda_i(\mathbf{x})$  in Eq. (64) provides the result.

APPENDIX C  
PROOF OF PROPOSITION 3

In this Appendix we prove the large system conditional MGFs given by Eqs. (22) and (23) and by Eqs. (24) and (25) in the IPC and TPC scenarios, respectively. We show the proof for the IPC case; differences with the TPC scenario will be underlined throughout the demonstration. We start by giving the definitions

$$\mathbf{p}_n \triangleq \frac{1}{\sqrt{K}} [ y_n \quad \mathbf{h}_{r,n} \mathbf{1}_K ]^t, \quad \mathbf{p} \triangleq [ \mathbf{p}_1^t \quad \cdots \quad \mathbf{p}_N^t ]^t, \quad (66)$$

with  $\mathbf{h}_{r,n}$  still denoting the  $n$ th row of  $\mathbf{H}$ . It can be noticed that  $\mathbf{p}_n | \mathbf{x} = \frac{1}{\sqrt{K}} \mathbf{v}_n | \mathbf{x}$ , where  $\mathbf{v}_n | \mathbf{x}$  has been defined in Eq. (60). Based on this observation, we can conclude that (i)  $\mathbf{p}_n | \mathbf{x}$ ,  $n \in \{1, \dots, N\}$ , are i.i.d. circularly complex Gaussian vectors (ii)  $\mathbb{E}\{\mathbf{p}_n | \mathbf{x}\} = \frac{1}{\sqrt{K}} \mathbb{E}\{\mathbf{v}_n | \mathbf{x}\} = \mathbf{0}_2$  and  $\check{\mathbf{R}} | \mathbf{x} \triangleq \mathbb{E}\{\mathbf{p}_n \mathbf{p}_n^\dagger | \mathbf{x}\} = \frac{1}{K} \mathbf{R} | \mathbf{x}$  (cf. Eq. (63)) and finally (iii)  $\mathbf{p} | \mathbf{x}$  is a circularly complex Gaussian vector, whose *characteristic function* (CF), denoted  $\Omega(\cdot)$ , can be expressed as a function of the dual vectors  $\bar{\mathbf{s}}_n \triangleq [ s_{1,n} \quad s_{2,n} ]^t \in \mathbb{C}^2$ ,  $n \in \{1, \dots, N\}$ , as follows [35]:

$$\Omega_{\mathbf{p}}(\bar{\mathbf{s}} | \mathbf{x}) = \exp \left[ -\frac{1}{4} \sum_{n=1}^N \bar{\mathbf{s}}_n^\dagger \cdot (\check{\mathbf{R}} | \mathbf{x}) \cdot \bar{\mathbf{s}}_n \right]. \quad (67)$$

By exploiting the structure of  $\check{\mathbf{R}} | \mathbf{x}$ , we can expand  $\Omega_{\mathbf{p}}(\bar{\mathbf{s}} | \mathbf{x})$  as follows

$$\Omega_{\mathbf{p}}(\bar{\mathbf{s}} | \mathbf{x}) = \exp \left[ -\frac{1}{K} \sum_{n=1}^N \Re\{s_{1,n}^* s_{2,n}\} \right]^{\ell(\mathbf{x})} \times \exp \left[ -\frac{1}{4} \sum_{n=1}^N \left( \|s_{1,n}\|^2 \cdot \left(1 + \frac{\sigma_w^2}{K}\right) + \|s_{2,n}\|^2 - 2\Re\{s_{1,n}^* s_{2,n}\} \right) \right] \quad (68)$$

W.l.o.g. we focus hereinafter on  $\Omega_{\mathbf{p}}(\bar{\mathbf{s}} | \mathcal{H}_1) = \sum_{\ell(\mathbf{x})=0}^K \Omega_{\mathbf{p}}(\bar{\mathbf{s}} | \ell(\mathbf{x})) P(\ell(\mathbf{x}) | \mathcal{H}_1)$  (since identical considerations apply to  $\Omega_{\mathbf{p}}(\bar{\mathbf{s}} | \mathcal{H}_0)$ ) and we recall that for the conditional i.i.d. sensor decisions  $\ell(\mathbf{x}) | \mathcal{H}_1 \sim \mathcal{B}(K, P_D)$ . Exploiting this assumption and Eq. (68), we get the explicit expression (we drop the dependence of  $\ell$  w.r.t.  $\mathbf{x}$ ):

$$\Omega_{\mathbf{p}}(\bar{\mathbf{s}} | \mathcal{H}_1) = \sum_{\ell=0}^K \binom{K}{\ell} P_D^\ell (1 - P_D)^{K-\ell} \exp \left[ -\frac{1}{K} \sum_{n=1}^N \Re\{s_{1,n}^* s_{2,n}\} \right]^\ell \exp \left[ -\frac{1}{4} \sum_{n=1}^N \left( \|s_{1,n}\|^2 \cdot \left(1 + \frac{\sigma_w^2}{K}\right) + \|s_{2,n}\|^2 - 2\Re\{s_{1,n}^* s_{2,n}\} \right) \right] \quad (69)$$

$$= \left( (1 - P_D) + P_D \exp \left[ -\frac{1}{K} \sum_{n=1}^N \Re\{s_{1,n}^* s_{2,n}\} \right] \right)^K \exp \left[ -\frac{1}{4} \sum_{n=1}^N \left( \|s_{1,n}\|^2 \cdot \left(1 + \frac{\sigma_w^2}{K}\right) + \|s_{2,n}\|^2 - 2\Re\{s_{1,n}^* s_{2,n}\} \right) \right] \quad (70)$$

Also, using table of limits, eventually we have that:

$$\begin{aligned} \bar{\Omega}_{\mathbf{p}}(\bar{\mathbf{s}} | \mathcal{H}_1) &\triangleq \lim_{K \rightarrow +\infty} \Omega_{\mathbf{p}}(\bar{\mathbf{s}} | \mathcal{H}_1) \\ &= \exp \left( -P_D \sum_{n=1}^N \Re\{s_{1,n}^* s_{2,n}\} \right) \times \\ &\quad \exp \left[ -\frac{1}{4} \sum_{n=1}^N \left( \|\bar{\mathbf{s}}_n\|^2 - 2\Re\{s_{1,n}^* s_{2,n}\} \right) \right] \\ &= \exp \left[ -\frac{1}{4} \sum_{n=1}^N \left( \|\bar{\mathbf{s}}_n\|^2 + 2 \cdot (2P_D - 1) \cdot \Re\{s_{1,n}^* s_{2,n}\} \right) \right]. \end{aligned} \quad (71) \quad (72) \quad (73)$$

It is worth noticing that  $\bar{\Omega}_{\mathbf{p}}(\bar{\mathbf{s}} | \mathcal{H}_1)$  in TPC scenario is obtained by setting  $\frac{1}{\text{SNR}} = \frac{\sigma_w^2}{K}$  in Eq. (70) and evaluating  $\lim_{K \rightarrow +\infty} \Omega_{\mathbf{p}}(\bar{\mathbf{s}} | \mathcal{H}_1)$  analogously. The expression in Eq. (73) can be recast as:

$$\begin{aligned} \bar{\Omega}_{\mathbf{p}}(\bar{\mathbf{s}} | \mathcal{H}_1) &= \exp \left[ -\sum_{n=1}^N \frac{1}{4} \bar{\mathbf{s}}_n^\dagger \cdot \bar{\mathbf{R}} \cdot \bar{\mathbf{s}}_n \right]; \\ \bar{\mathbf{R}} &\triangleq \begin{bmatrix} 1 & 2P_D - 1 \\ 2P_D - 1 & 1 \end{bmatrix}. \end{aligned} \quad (74) \quad (75)$$

Such a result, when compared with Eq. (67) and with the use of *Levi's continuity theorem* [36], states that when  $K \rightarrow +\infty$ ,  $\mathbf{p}_n | \mathcal{H}_1$ ,  $n \in \{1, \dots, N\}$ , are i.i.d and  $\mathbf{p}_n | \mathcal{H}_1 \xrightarrow{d} \mathcal{N}_{\mathbb{C}}(\mathbf{0}_2, \bar{\mathbf{R}})$ . Analogously, in the TPC scenario a similar result holds when  $\bar{\mathbf{R}}$  is appropriately replaced. Finally, this information is readily exploited by considering that  $\tilde{\Lambda} \triangleq \frac{1}{K} \Lambda_{MRC}$  equals to

$$-\tilde{\Lambda} = \sum_{n=1}^N \mathbf{p}_n^\dagger \cdot \mathbf{F} \cdot \mathbf{p}_n, \quad (76)$$

where  $\mathbf{F}$  has the same definition as in Eq. (60). Therefore, as  $K \rightarrow +\infty$ ,  $-\tilde{\Lambda} | \mathcal{H}_1$  is a sum of Hermitian quadratic forms of i.i.d. circularly complex Gaussian vectors whose MGF is easily derived using similar arguments as in Appendix B, thus providing Eqs. (22) and (23) (and analogously Eqs. (24) and (25)).

APPENDIX D  
PROOF OF PROPOSITION 4

The first step in proving Eq. (28) is showing that, after some manipulations, the AUC defined in Eq. (26) for a generic statistic  $\Lambda$  can be expressed in the alternative form:

$$\text{AUC} = \int_{-\infty}^{+\infty} P_{D_0}(\gamma) p_{-\Lambda}(-\gamma | \mathcal{H}_0) d\gamma \quad (77)$$

where  $p_{-\Lambda}(\lambda | \mathcal{H}_i)$ ,  $\mathcal{H}_i \in \mathcal{H}$ , denotes the conditional pdf of  $-\Lambda$ . Furthermore, it can be shown that the Laplace transforms of  $P_{D_0}(\gamma)$  and  $p_{-\Lambda}(-\gamma | \mathcal{H}_0)$  are given by  $\frac{\Phi_{-\Lambda}(-s | \mathcal{H}_1)}{-s}$  and  $\Phi_{-\Lambda}(-s | \mathcal{H}_0)$ , respectively. Also, let us recall the relationship between a generic function  $g(\lambda)$  and its two-sided Laplace transform  $\Phi_g(s) \triangleq \int_{-\infty}^{+\infty} g(\lambda) \exp(-\lambda s) ds$

$$\lim_{s \rightarrow 0} \Phi_g(s) = \int_{-\infty}^{+\infty} g(\lambda) d\lambda, \quad (78)$$

and the property relating the Laplace transform of the product of two generic functions  $a(\lambda)$  and  $b(\lambda)$

$$\Phi_{a \cdot b}(s) = \frac{1}{2\pi j} \int_{\alpha-j\infty}^{\alpha+j\infty} \Phi_a(p)\Phi_b(s-p)dp. \quad (79)$$

where  $\alpha$  is a constant that ensures that the integration is performed in the RC of  $\Phi_a(p)$ . Combining Eqs. (78) and (79) we get

$$\frac{1}{2\pi j} \int_{\alpha-j\infty}^{\alpha+j\infty} \Phi_a(p)\Phi_b(-p)dp = \int_{-\infty}^{+\infty} a(\lambda)b(\lambda)d\lambda. \quad (80)$$

The obtained expression is now used to evaluate Eq. (77) in the Laplace domain. In fact, exploiting the explicit expressions of the Laplace transforms of  $P_{D_0}(\gamma)$  and  $p_{-\Lambda}(-\gamma|\mathcal{H}_0)$  in Eq. (80) we obtain

$$\text{AUC} = \frac{1}{2\pi j} \int_{\alpha-j\infty}^{\alpha+j\infty} \frac{\Phi_{-\Lambda}(-p|\mathcal{H}_1)}{-p} \Phi_{-\Lambda}(p|\mathcal{H}_0)dp, \quad (81)$$

where we can choose  $\alpha = -c_1$ , where  $c_1$  has the same meaning as in Eq. (16), i.e. belongs to the positive restriction of the RC of  $\Phi_{-\Lambda}(s|\mathcal{H}_1)$ . Finally, the substitution  $s^* = -p$  in Eq. (81) gives the result in Eq. (28).

## REFERENCES

- [1] B. Chen, R. Jiang, T. Kasetkasem, and P. K. Varshney, "Channel aware decision fusion in wireless sensor networks," *IEEE Trans. Signal Process.*, vol. 52, no. 12, pp. 3454–3458, Dec. 2004.
- [2] B. Chen, L. Tong, and P. K. Varshney, "Channel-aware distributed detection in wireless sensor networks," *IEEE Signal Process. Mag.*, vol. 23, no. 4, pp. 16–26, Jul. 2006.
- [3] A. Lei and R. Schober, "Coherent Max-Log decision fusion in wireless sensor networks," *IEEE Trans. Commun.*, vol. 58, no. 5, pp. 1327–1332, May 2010.
- [4] W. Li and H. Dai, "Distributed detection in wireless sensor networks using a multiple access channel," *IEEE Trans. Signal Process.*, vol. 55, no. 3, pp. 822–833, Mar. 2007.
- [5] C. R. Berger, M. Guerriero, S. Zhou, and P. K. Willett, "PAC vs. MAC for decentralized detection using noncoherent modulation," *IEEE Trans. Signal Process.*, vol. 57, no. 9, pp. 3562–3575, Sep. 2009.
- [6] F. Li, J. S. Evans, and S. Dey, "Decision fusion over noncoherent fading multiaccess channels," *IEEE Trans. Signal Process.*, vol. 59, no. 9, pp. 4367–4380, Sep. 2011.
- [7] D. Ciuonzo, G. Romano, and P. Salvo Rossi, "Optimality of received energy in decision fusion over Rayleigh fading diversity MAC with non-identical sensors," *IEEE Trans. Signal Process.*, vol. 61, no. 1, pp. 22–27, Jan. 2013.
- [8] K. Umebayashi, J. J. Lehtomaki, T. Yazawa, and Y. Suzuki, "Efficient decision fusion for cooperative spectrum sensing based on OR-rule," *IEEE Trans. Wireless Commun.*, vol. 11, no. 7, pp. 2585–2595, Jul. 2012.
- [9] S. Yiu and R. Schober, "Nonorthogonal transmission and noncoherent fusion of censored decisions," *IEEE Trans. Veh. Technol.*, vol. 58, no. 1, pp. 263–273, Jan. 2009.
- [10] X. Zhang, H. V. Poor, and M. Chiang, "Optimal power allocation for distributed detection over MIMO channels in wireless sensor networks," *IEEE Trans. Signal Process.*, vol. 56, no. 9, pp. 4124–4140, Sep. 2008.
- [11] K. Bai and C. Tepedelenlioglu, "Distributed detection in UWB wireless sensor networks," *IEEE Trans. Signal Process.*, vol. 58, no. 2, pp. 804–813, Feb. 2010.
- [12] M. K. Banavar, A. D. Smith, C. Tepedelenlioglu, and A. Spanias, "On the effectiveness of multiple antennas in distributed detection over fading MACs," *IEEE Trans. Wireless Commun.*, vol. 11, no. 5, pp. 1744–1752, May 2012.
- [13] D. Ciuonzo, G. Romano, and P. Salvo Rossi, "Channel-aware decision fusion in distributed MIMO wireless sensor networks: Decode-and-fuse vs. decode-then-fuse," *IEEE Trans. Wireless Commun.*, vol. 11, no. 8, pp. 2976–2985, Aug. 2012.
- [14] B. Picinbono, "On deflection as a performance criterion in detection," *IEEE Trans. Aerosp. Electron. Syst.*, vol. 31, no. 3, pp. 1072–1081, Jul. 1995.
- [15] S. M. Kay, *Fundamentals of Statistical Signal Processing, Volume 2: Detection Theory*. Prentice Hall PTR, Jan. 1998.
- [16] M. Biguesh and A. B. Gershman, "Training-based MIMO channel estimation: a study of estimator tradeoffs and optimal training signals," *IEEE Trans. Signal Process.*, vol. 54, no. 3, pp. 884–893, 2006.
- [17] T. L. Marzetta, "Noncooperative cellular wireless with unlimited numbers of base station antennas," *IEEE Trans. Wireless Commun.*, vol. 9, no. 11, pp. 3590–3600, Nov. 2010.
- [18] P. K. Varshney, *Distributed Detection and Data Fusion*, 1st ed. Springer-Verlag New York, Inc., 1996.
- [19] E. Biglieri, G. Caire, G. Taricco, and J. Ventura-Traveset, "Simple method for evaluating error probabilities," *Electronics Letters*, vol. 32, no. 3, pp. 191–192, Feb. 1996.
- [20] A. Annamalai, C. Tellambura, and V. K. Bhargava, "Efficient computation of MRC diversity performance in Nakagami fading channel with arbitrary parameters," *Electronics Letters*, vol. 34, no. 12, pp. 1189–1190, Jun. 1998.
- [21] E. Biglieri, G. Caire, G. Taricco, and J. Ventura-Traveset, "Computing error probabilities over fading channels: A unified approach," *Eur. Trans. on Telecomm.*, vol. 9, no. 1, pp. 15–25, Jan. 1998.
- [22] A. Dembo and O. Zeitouni, *Large Deviations Techniques and Applications*. Jones and Bartlett, 1993.
- [23] D. J. Love and R. W. Heath Jr., "Equal gain transmission in multiple-input multiple-output wireless systems," *IEEE Trans. Commun.*, vol. 51, no. 7, pp. 1102–1110, Jul. 2003.
- [24] A. P. Bradley, "The use of the area under the ROC curve in the evaluation of machine learning algorithms," *Pattern Recognition*, vol. 30, no. 7, pp. 1145–1159, 1997.
- [25] S. Atapattu, C. Tellambura, and H. Jiang, "Analysis of area under the ROC curve of energy detection," *IEEE Trans. Wireless Commun.*, vol. 9, no. 3, pp. 1216–1225, Mar. 2010.
- [26] —, "MGF based analysis of area under the ROC Curve in energy detection," *IEEE Commun. Lett.*, vol. 15, no. 12, pp. 1301–1303, Dec. 2011.
- [27] T. Fawcett, "ROC graphs: Notes and practical considerations for researchers," HP Laboratories, MS 1143, 1501 Page Mill Road, Palo Alto, CA 94304, Tech. Rep. HPL-2003-4, Mar. 2004.
- [28] H. H. Barrett, C. K. Abbey, and E. Clarkson, "Objective assessment of image quality. III. ROC metrics, ideal observers, and likelihood-generating functions," *Journal of Optical Society of America A*, vol. 15, no. 6, pp. 1520–1535, Jun. 1998.
- [29] Z. Quan, S. Cui, and A. H. Sayed, "Optimal linear cooperation for spectrum sensing in cognitive radio networks," *IEEE J. Sel. Topics Signal Process.*, vol. 2, no. 1, pp. 28–40, Feb. 2008.
- [30] M. Schwarz, W. R. Bennet, and S. Stein, *Communication Systems and Techniques*. New York: McGraw-Hill, 1966.
- [31] S. Boyd and L. Vandenberghe, *Convex Optimization*. New York, NY, US: Cambridge University Press, 2004.
- [32] P. J. Schreier and L. L. Scharf, *Statistical Signal Processing of Complex-Valued Data: The Theory of Improper and Noncircular Signal*. Cambridge, 2010.
- [33] Y. Bar-Shalom, T. Kirubarajan, and X. R. Li, *Estimation with Applications to Tracking and Navigation*. New York, NY, USA: John Wiley & Sons, Inc., 2002.
- [34] X. Zhu and R. D. Murch, "Performance analysis of maximum likelihood detection in a MIMO antenna system," *IEEE Trans. Commun.*, vol. 50, no. 2, pp. 187–191, Feb. 2002.
- [35] B. Picinbono, "Second-order complex random vectors and normal distributions," *IEEE Trans. Signal Process.*, vol. 44, no. 10, pp. 2637–2640, Oct. 1996.
- [36] A. F. Karr, *Probability*. Springer-Verlag New York, Inc., 1993.